Geochemistry Geophysics Geosystems G3
AN ELECTRONIC JOURNAL OF THE EARTH SCIENCES
Published by AGU and the Geochemical Society

Article
Volume 10, Number 12
8 December 2009
Q12006, doi:10.1029/2009GC002874
ISSN: 1525-2027

An $^{40}Ar/^{39}Ar$ geochronology on a mid-Eocene igneous event on the Barton and Weaver peninsulas: Implications for the dynamic setting of the Antarctic Peninsula

Fei Wang and Xiang-Shen Zheng
Paleomagnetism and Geochronology Laboratory, State Key Laboratory of Lithospheric Evolution, Institute of Geology and Geophysics, Chinese Academy of Sciences, Beijing 100029, China (wangfei@mail.iggcas.ac.cn)

Jong I. K. Lee and Won Hie Choe
Korea Polar Research Institute, KORDI, Songdo Techno Park, 7-50, Incheon 406-840, South Korea

Noreen Evans
CSIRO Exploration and Mining, 26 Dick Perry Avenue, Kensington, Western Australia 6151, Australia

Also at John de Laeter Centre of Mass Spectrometry, Department of Applied Geology, Curtin University of Technology, Perth, Western Australia 6845, Australia

Ri-Xiang Zhu
Paleomagnetism and Geochronology Laboratory, State Key Laboratory of Lithospheric Evolution, Institute of Geology and Geophysics, Chinese Academy of Sciences, Beijing 100029, China

[1] The genesis of basaltic to andesitic lavas, mafic dikes, and granitoid plutons composing the subaerial cover on the Barton and Weaver peninsulas, Antarctica, is related to arc formation and subduction processes. Precise dating of these polar rocks using conventional $^{40}Ar/^{39}Ar$ techniques is compromised by the high degree of alteration (with loss on ignition as high as 8%). In order to minimize the alteration effects we have followed a sample preparation process that includes repeated acid leaching, acetone washing, and hand picking, followed by an overnight bake at 250°C. After this procedure, groundmass samples can yield accurate age plateaus consisting of 70%–100% of the total $^{39}Ar_k$ released using high-resolution heating schedules. The different rock types studied on the Barton and Weaver peninsulas yielded almost coeval ages, suggesting a giant igneous event in the Weaver and Barton peninsulas at 44.5 Ma. A compilation of newly published ages indicate that this event took place throughout the whole South Shetland Islands, suggesting a dynamic incident occurred at this stage during the arc evolution history. We related this igneous event to a mantle delamination mechanism during Eocene times. The delamination process began at ~52 Ma, and the resultant upwelling of asthenosphere baffled the subduction of Phoenix plate, causing an abrupt decrease in convergence rate. Then multiple magmatic sources were triggered, resulting in a culminating igneous activity during 50–40 Ma with a peak at ~45 Ma along the archipelago. The delamination also caused the extension regime indicated by the dike swarm, plugs and sills all over the archipelago, and the uplift of Smith metamorphic complex and Livingston Island. Delamination process may have finished at some time during 40–30 Ma, leaving a weak igneous activity at that stage and thereafter. The convergence rate then recovered gradually, as indicated by the magnetic anomaly identifications. This model is supported by seismic observation of deep velocity anomalies beneath the Antarctic Peninsula.

Components: 16,331 words, 13 figures, 4 tables.

Keywords: $^{40}Ar/^{39}Ar$ geochronology; igneous event; geodynamics; delamination; Antarctic.

Index Terms: 1115 Geochronology: Radioisotope geochronology; 1135 Geochronology: Correlative geochronology.

Received 23 September 2009; **Accepted** 21 October 2009; **Published** 8 December 2009.

Wang, F., X.-S. Zheng, J. I. K. Lee, W. H. Choe, N. Evans, and R.-X. Zhu (2009), An $^{40}Ar/^{39}Ar$ geochronology on a mid-Eocene igneous event on the Barton and Weaver peninsulas: Implications for the dynamic setting of the Antarctic Peninsula, *Geochem. Geophys. Geosyst.*, *10*, Q12006, doi:10.1029/2009GC002874.

1. Introduction

[2] It has long been noticed that the Paleocene-Eocene is the major period of igneous activity on the South Shetland Islands, Antarctic peninsula [e.g., *Pankhurst and Smellie*, 1983; *Smellie et al.*, 1984; *Birkenmajer et al.*, 1986; *Smellie et al.*, 1996; *Willan and Kelley*, 1999; *Zheng et al.*, 2003; *Kraus*, 2005; *Kamenov et al.*, 2005], but when and how is still a dispute so far. Although the geochronological researches on Antarctica peninsula started almost a half century ago, more recent studies showed that almost half of those early ages on the South Shetland Islands are unreliable due to either Ar and K loss associated with alteration, or excess argon presence [*Willan and Kelley*, 1999; *Kraus*, 2005]. For the same reason, the migration trend of volcanism from SW to NE [*Pankhurst and Smellie*, 1983; *Birkenmajer*, 1994] and related model of counter clockwise rotation of the Antarctic plate over a stationary hot spot [*Birkenmajer*, 1994] was challenged [*Willan and Kelley*, 1999]. Although more precise dating results have been published recently [*Willan and Kelley*, 1999; *Zheng et al.*, 2003; *Kraus*, 2005; *Kamenov et al.*, 2005], there is still a paucity of age information on the archipelago, especially in the central part of it. Precise dates are still in need in order to constrain the regional trends better.

[3] Barton and Weaver peninsulas are located in the SW end of the King George Island. It still remains unclear what stage is responsible for the major igneous activity on these peninsulas. Here we report the first comprehensive precise dating results on a wide spectrum of rock types, including basalt, basaltic andesite, propylite, mafic dike, granodiorite and diorite, in order to understand the sequence of igneous activity in this locality. We try to relate the dating results to the whole evolution history of the archipelago in plate tectonics.

[4] We elaborate the $^{40}Ar/^{39}Ar$ method and spend efforts on the dating of these highly altered polar volcanics. Alteration processes may lead to loss of radiogenic Ar ($^{40}Ar^*$) from original phases and/or addition of potassium to the secondary alteration phases [*Roddick*, 1978; *Seidemann*, 1988; *Foland et al.*, 1993; *Koppers et al.*, 2000]. Recoil effects of nucleogenic isotopes during irradiation would be enhanced due to alteration [*Turner and Cadogan*, 1974; *Dalrymple and Clague*, 1976; *Seidemann*, 1977, 1978; *Walker and McDougall*, 1982], resulting in lose some $^{39}Ar_k$ and $^{37}Ar_{Ca}$ from very fine grained volcanic phases and secondary minerals.

[5] The occurrence of alteration phases in the Antarctic volcanics diminishes the suitability of whole rock dating by conventional K/Ar methods [e.g., *Pankhurst and Smellie*, 1983; *Park*, 1989; *Smellie et al.*, 1996; *Willan and Kelley*, 1999; *Kim et al.*, 2000], and by the $^{40}Ar/^{39}Ar$ step-heating method to a great extent [e.g., *Park*, 1989; *Willan and Kelley*, 1999; *Kim et al.*, 2000; *Zheng et al.*, 2000]. One approach to the problems is the selection of unaltered phenocryst phases for dating. However, research has shown that phenocrysts could retain inherited ^{40}Ar and excess ^{40}Ar that was accumulated during crystallization in the magmatic chamber [e.g., *McDougall and Harrison*, 1999; *Wang et al.*, 2008]. Dating of crystallized groundmass separates by the $^{40}Ar/^{39}Ar$ step-heating technique is another approach that is widely used for mafic volcanic rocks [e.g., *McDougall and Harrison*, 1999; *Koppers et al.*, 2000; *Koppers and Staudigel*, 2003; *Wang et al.*, 2006a, 2006b].

2. Geological Setting and Samples

[6] During our expedition in 2005 to the South Shetland Islands, Antarctica, a geological survey was carried out and samples of igneous rocks from the Barton and Weaver peninsulas were collected.

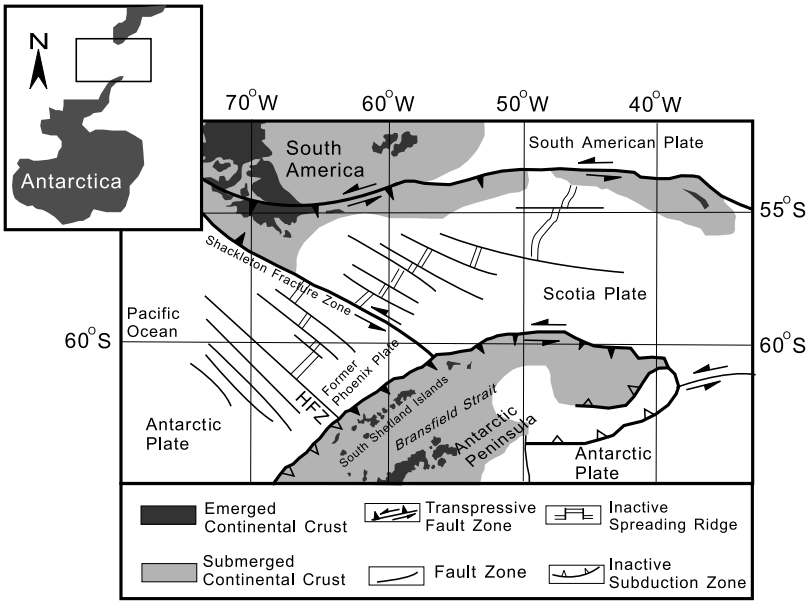

Figure 1. Tectonic sketch map of the study area. Modified from *Galindo-Zaldívar et al.* [2004].

[7] The South Shetland Islands, a 300 km long Jurassic-Quaternary magmatic island arc northwest of the Antarctic Peninsula, form the northwest edge of the Antarctic continent (Figure 1). The island arc is seated on a basement of schist, gneiss and deformed sedimentary rocks and is separated from the Antarctic Peninsula by the Bransfield Strait. The Bransfield Basin is asymmetrical, with most of the sediment input coming from the passive Antarctic Peninsula margin [*Galindo-Zaldívar et al.*, 2004].

[8] The Scotia and Antarctic Plates, the two major plates in the region, connect via a left-lateral transpressive fault zone located along the Scotia Ridge (Figure 1). The northwest segment of the fault zone (known as the Shackleton Fracture Zone), cuts through a submarine ridge separating the South Chill trench and the South Shetland fore arc. The southeast end of the fault zone is subducted beneath the South Shetland fore arc along with the former Phoenix Plate [*Pelayo and Wiens*, 1989; *Aldaya and Madonado*, 1996; *Galindo-Zaldívar et al.*, 2004]. The subduction of the former Phoenix Plate caused the collision of the ridge crest with the trench of the South Shetland Islands beginning in late Paleocene time [*Maldonado et al.*, 2000]. Later incorporation of the Phoenix Plate into the Antarctic Plate caused the cessation of subduction [*Barker*, 1982; *Maldonado et al.*, 1994], sometime after magnetic chron C2A (3.3 ± 0.2 Ma) [*Lawver et al.*, 1992; *Livermore et al.*, 2000; *Maldonado et al.*, 2000]. Some geochronology along the South Shetland Islands suggest that the oblique subduction of Phoenix Plate came to an end progressively northeastward as a result of ridge-trench collision [*Pankhurst and Smellie*, 1983].

[9] King George Island is the largest of the South Shetland Islands, consisting mainly of subalkaline volcanic and plutonic rocks of Paleocene to Eocene age (Figure 2) [*Smellie et al.*, 1984]. The Barton and Weaver peninsulas form the Marian cove in the southwest portion of King George Island (Figure 2). The lithology of the Barton and Weaver peninsulas comprises lavas, pyroclastics, hypabyssal and plutonic rocks (Figure 2). The Lower Volcanic Member [*Davis*, 1982], later named the Sejong Formation [*Yoo et al.*, 2001], is distributed along the southern and southwestern coasts of Barton Peninsula, and in most parts of the Weaver Peninsula (Figure 2). It is largely composed of volcaniclasts with a maximum thickness of about 100 m [*Yeo et al.*, 2004]. Late Paleocene to Eocene deposition ages were suggested by plant fossil leaves in fine-grained sandstones [*Yoo et al.*, 2001]. Above the Sejong Formation lies the mafic to intermediate volcanic lavas in Barton Peninsula.

[10] Basalt and basaltic andesite show a prophyritic texture with predominant plagioclase phenocrysts. Clinopyroxene and orthopyroxene also occur as minor phenocrysts. Holocrystalline groundmass commonly shows flow texture with preferred orientation microlite. The eruption ages of these lavas were constrained during Paleocene to Eocene mostly based on the K-Ar whole rock methods [*Pankhurst and Smellie*, 1983; *Park*, 1989; *Kim et al.*, 2000; *Hur et al.*, 2001]. However, two early

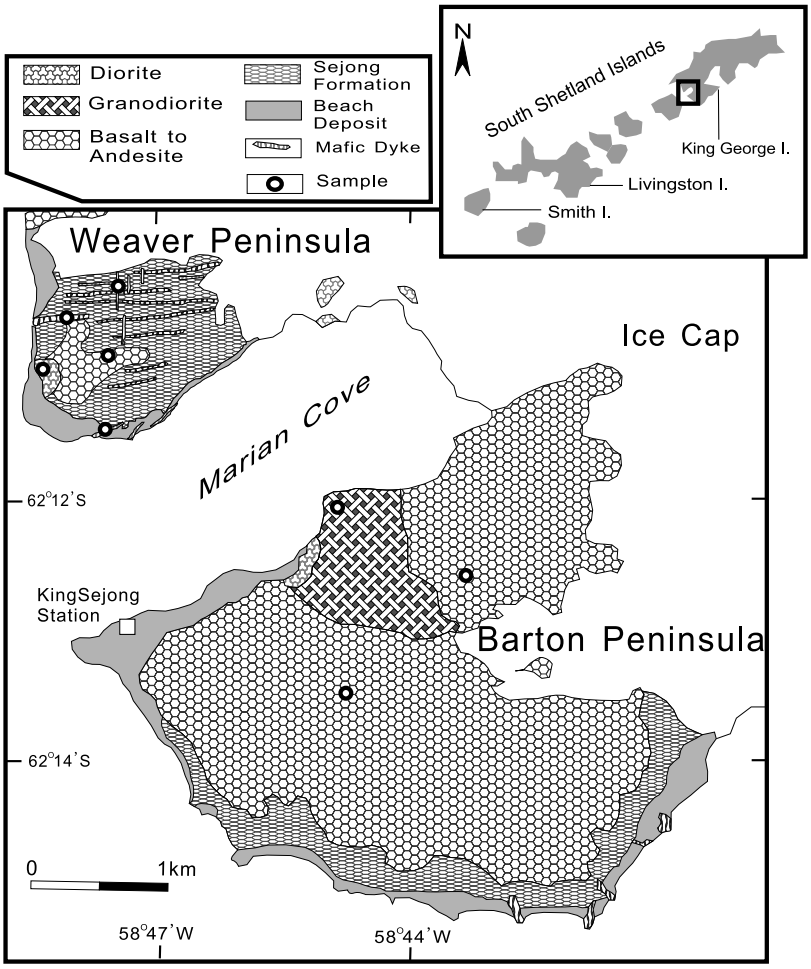

Figure 2. Geological map of Barton and Weaver peninsulas, King George Island, Antarctica (modified from *Lee et al.* [2002]). The sample sites are marked.

Cretaceous ages determined by $^{40}Ar/^{39}Ar$ whole rock methods were reported on the basalt in Barton Peninsula (119–120 Ma [*Zheng et al.*, 2000]).

[11] Mafic dikes are widely distributed in the Weaver Peninsula and coastal area of the Barton Peninsula (Figure 2). In the Weaver Peninsula, east-west trending mafic dikes are cut by north-south trending dikes. They are generally plagioclase-phyric and clinopyroxene-phyric basalts 1–5 m in width and several hundred to thousand meters long. There has been no emplacement age reported for these dikes prior to this work.

[12] A coarse-grained granodioritic pluton occurs in the northern Barton Peninsula with reported whole rock K-Ar ages of 42–45 Ma [*Park*, 1989], biotite K-Ar ages of 41.9 ± 0.9 Ma and 41.2 ± 0.9 Ma [*Lee et al.*, 1996], and a $^{40}Ar/^{39}Ar$ whole rock age of 48.4 ± 05 Ma [*Zheng et al.*, 2000]. A small stock of diorite intruded into the Sejong Formation on Weaver Peninsula and a whole rock $^{40}Ar/^{39}Ar$ age of 48.4 ± 0.5 Ma [*Kim et al.*, 2000] was reported for this pluton. The granodiorite consists of alkali feldspar, plagioclase, hornblende, biotite and quartz and Fe-Ti oxides, whereas the diorite is composed mainly of plagioclase, biotite, hornblende, alkali feldspar, Fe-Ti oxides and minor quartz.

[13] Alteration is prominent in the rocks. The most common alteration minerals are calcite, chlorite and sericite, and less frequently also epidote, albite, quartz and zeolite. A high loss on ignition (LOI) value characterizes most of the volcanic rock samples studied (Table 1). LOI represents the volatile content (in weight percent) released by the sample during heating and is a useful indicator of the degree of alteration [*Kraus*, 2005]. The higher the LOI value, the stronger the alteration of the sample. Conventionally, LOI values <3 indicate relatively fresh rocks, whereas samples with an LOI > 4 are interpreted as altered. However, it has been emphasized, that in general primary subduction zone magmas contain higher and more variable volatile

Table 1. Geochemical Compositions and Sr and Nd Isotopes

	Sample and Rock							
	05121804, Andesite	05121903, Mafic Dike	05121908, Mafic Dike	05122401, Diorite	05122402, Basalt	05122408, Mafic Dike	05122602, Granodiorite	05122605, Propylite
Major Elements (wt %, by XRF)								
SiO_2	49.81	50.77	49.04	51.01	45.47	47.46	62.28	48.75
Al_2O_3	18.46	16.59	18.51	19.01	17.22	18.01	16.36	24.03
TiO_2	0.70	0.58	0.80	0.71	0.63	0.67	0.54	1.06
TFe_2O_3	9.00	7.93	8.62	8.54	9.20	8.16	5.42	11.95
MnO	0.15	0.13	0.15	0.15	0.14	0.12	0.10	0.26
MgO	5.80	2.88	4.82	4.00	6.03	2.90	2.50	3.72
CaO	8.24	9.45	10.41	6.80	11.90	10.35	4.65	2.38
Na_2O	3.48	2.49	2.49	4.97	1.67	2.36	3.89	1.80
K_2O	0.59	0.60	0.80	1.12	0.70	1.28	2.73	3.23
P_2O_5	0.13	0.17	0.19	0.21	0.11	0.13	0.14	0.12
LOI	3.22	8.27	3.88	3.20	7.15	8.14	0.82	2.16
TOTAL	99.58	99.86	99.71	99.72	99.59	99.58	99.43	99.46
Trace Elements (ppm, by ICP-MS)								
Li	10.33	44.61	20.89	14.59	13.43	26.15	13.43	12.06
Be	0.594	0.781	0.73	0.97	1.42	1.04	1.42	1.32
Sc	25.39	18.98	29.99	14.06	15.64	28.49	15.64	26.33
V	262.84	194.00	282.06	209.89	242.04	266.36	142.04	250.45
Cr	25.00	12.51	13.33	6.85	14.45	11.91	14.45	21.66
Co	22.64	20.30	29.00	21.43	14.53	25.79	14.53	39.11
Ni	17.89	5.90	6.70	2.25	4.18	30.98	4.18	10.65
Cu	72.73	77.50	144.08	100.70	56.58	129.05	56.58	393.04
Zn	70.34	58.63	73.19	80.20	62.56	76.51	62.56	183.00
Ga	18.32	16.65	19.72	19.89	18.44	19.63	18.44	26.61
Rb	11.52	20.15	17.04	20.02	63.70	26.55	63.70	85.80
Sr	551.48	651.06	552.41	748.20	399.81	566.05	399.81	294.14
Y	12.41	11.66	14.44	14.80	25.21	13.03	25.21	22.33
Zr	49.47	64.28	60.10	83.29	195.76	70.05	195.76	211.43
Nb	1.65	1.54	1.94	2.66	4.17	1.86	4.17	4.33
Rare Earth Elements (ppm, by ICP-MS)								
La	6.14	16.74	9.18	11.67	7.62	10.90	22.94	20.74
Ce	13.21	33.58	20.18	27.86	17.89	23.73	51.08	53.68
Pr	2.18	4.20	3.16	3.82	2.36	3.37	6.87	7.78
Nd	9.93	16.09	13.49	15.97	11.33	14.02	27.68	29.94
Sm	2.77	3.62	3.46	4.07	2.94	3.63	6.51	7.11
Eu	0.96	1.06	1.13	1.26	1.11	1.18	1.21	2.40
Gd	2.65	2.78	3.24	3.51	3.10	3.08	5.43	5.55
Tb	0.42	0.39	0.49	0.53	0.52	0.45	0.82	0.79
Dy	2.50	2.24	2.95	3.14	2.90	2.58	4.80	4.44
Ho	0.51	0.43	0.56	0.61	0.62	0.50	0.98	0.90

Table 1. (continued)

	Sample and Rock							
	05121804, Andesite	05121903, Mafic Dike	05121908, Mafic Dike	05122401, Diorite	05122402, Basalt	05122408, Mafic Dike	05122602, Granodiorite	05122605, Propylite
Er	1.44	1.19	1.58	1.70	1.60	1.38	2.75	2.54
Tm	0.21	0.17	0.23	0.24	0.25	0.21	0.43	0.38
Yb	1.38	1.14	1.52	1.63	1.62	1.34	2.84	2.50
Lu	0.20	0.17	0.23	0.24	0.24	0.20	0.44	0.38
				Sr and Nd Isotopes				
$(^{87}Sr/^{86}Sr)_i$, $\pm 2\sigma$	0.703609, ±12	0.703342, ±15	0.703877, ±13	0.703534, ±14	0.703396, ±15	0.703508, ±11	0.703506, ±9	0.703560, ±16
$[^{143}Nd/^{144}Nd]_i$, $\pm 2\sigma$	0.512873, ±10	0.512891, ±7	0.512867, ±5	0.512956, ±4	0.512858, ±9	0.512897, ±3	0.512861, ±6	0.512875, ±4
εNd[45 Ma]	5.7	6.1	5.6	7.3	5.4	6.2	5.5	5.8

contents (0–4 wt %) than magmas from other tectonic settings [*Tatsumi and Eggins*, 1995; *Kraus*, 2005].

[14] According to microscopic observations, alteration of anorthite to sericite and chlorite has been observed in many samples. Concerning plagioclase, partial or complete alteration of anorthite-rich cores to sericite and chlorite leads to so-called "filled plagioclase" (Figure 3a, 05121903). This phenomenon is due to the albite-rich rime having a higher resistance against hydrothermal alteration than the anorthite-richer interior of the crystal, causing an earlier breakdown of the latter. Orthopyroxene characterizes with opacitization, a process starting along fractures within the crystal (Figure 3b, 05122402), leading to complete disintegration under formation of opaque Fe minerals finally. Calcite tends to form fillings of amygdales from disintegrating phenocryst (plagioclase and pyroxene). Chlorite and sericite derive mainly from alteration of plagioclase, forming the filling of phenocrysts that have an albite-rich rim, but are also evenly distributed in the matrix. Epidote and clinozoisite and quartz occur often in paragenesis with calcite and chlorite as fillings of amygdales, of fractures within plagioclase phenocrysts.

3. Methodology

3.1. Major and Trace Elements and Sr and Nd Isotopes

[15] Major element abundance was determined using X-ray fluorescence spectrometry (XRF) with a Philips PW1400 spectrometer at IGGCAS (Institute of Geology and Geophysics, Chinese Academy of Sciences). Analytical uncertainties range from 2% to 5%. Trace elements including REE elements were analyzed using ICP-MS (IGGCAS), with analytical uncertainties less than 5%.

[16] For Sr, Nd isotopic analyses (IGGCAS) the concentrations of Rb, Sr, Sm and Nd were obtained by using isotope dilution using a mixed ^{87}Rb-^{84}Sr-^{149}Sm-^{150}Nd spike solution. Isotopic ratio measurements were made on a multicollector MAT-262 thermal ionization mass spectrometer. Measured Sr isotope ratios were normalized to $^{86}Sr/^{88}Sr = 0.1194$; the $^{87}Sr/^{86}Sr$ of the Sr standard NBS-607 was 1.200393 ± 12 (2σ, n = 6). Measured Nd ratios were normalized to $^{144}Nd/^{146}Nd = 0.7219$; the average value of the $^{143}Nd/^{144}Nd$ ratios of La Jolla standard is 0.511863 ± 7 (2σ, n = 6). Analytical uncertainties are estimated to be <0.5%–1.0% for both $^{87}Rb/^{86}Sr$ and $^{147}Sm/^{144}Nd$

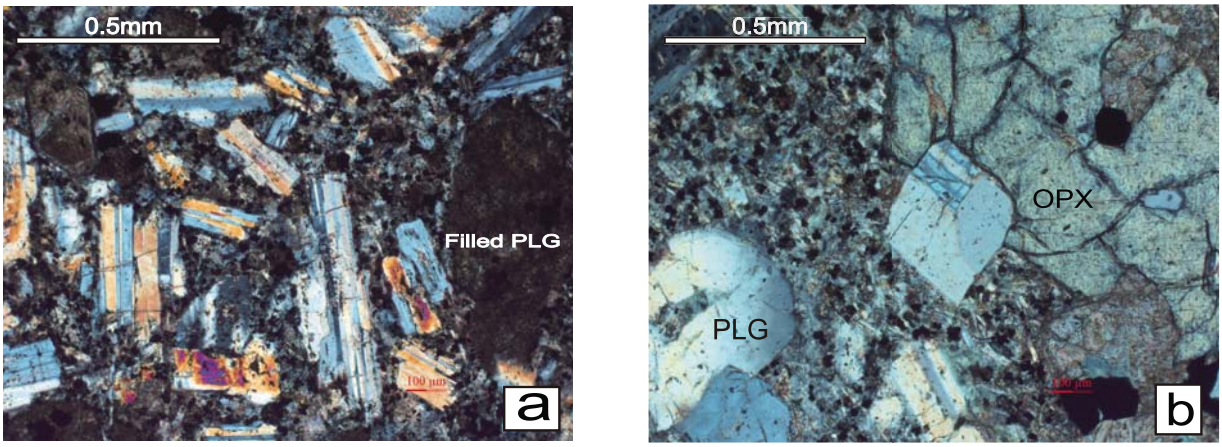

Figure 3. (a) Dike sample 05121908 shows alteration to microcrystalline mixture of sericite and chlorite. "Filled plagioclase" was formed from a plagioclase phenocryst. (b) Basalt sample 05122402 shows beginning of opacitization along fractures in an orthopyroxene phenocryst.

ratios. Blanks during the course of this study averaged 0.4 ng for Rb, 0.2 ng for Sr, 0.06 ng for Sm and 0.05 ng for Nd. For plotting on a diagram, the Sr and Nd isotope ratios were corrected to 45 Ma.

3.2. The $^{40}Ar/^{39}Ar$ Analyses

3.2.1. Sample Preparation and Irradiation

[17] Six groundmass samples were obtained from basalt, basaltic andesite and propylite samples collected from lavas as well as mafic dikes, and two K-feldspar separates were selected from granidiorite and diorite samples. During sample preparation, we attempted to minimize the quantity of alteration products obtained by following the methods of *Koppers et al.* [2000]. The samples were crushed in a steel jaw crusher followed by grinding in a steel mill. Grinding was accomplished in 1–2 s time steps and alternated with sieving at 200 μm until 90% of the rock powder was reduced to <200 μm. The remaining 280–200 μm fraction included the hardest components of the altered samples and are, by assumption, the freshest parts of the samples. The groundmass aliquots were then hand picked under a binocular microscope from these 200–280 μm fractions. The aliquots of every groundmass sample were inspected carefully to remove phenocrysts or xenocrysts, and all other impurities.

[18] Two K-feldspar separates from the granodiorite rock from Barton Peninsula and the diorite sample from Weaver Peninsula were obtained. Following the crushing and sieving procedures described above, the 280–450 μm fractions were processed by heavy liquid separation and then by magnetic separation using a Frantz magnetic separator to select the K-feldspar. The fresh, clear K-feldspar crystals, without visible impurities, connections or altered grains were selected by hand picking under a binocular microscope.

[19] The separates of groundmass and K-feldspar were further cleaned by acid leaching with 2 N HNO_3 for 30 min in an ultrasonic bath, heated to 50°C in order to remove the calcite and other nitric-soluble phases. The leached separates were washed in an ultrasonic bath in deionized water three times, each for 30 min, and then in acetone three times (for 30 min), and dried in preparation for irradiation.

[20] All aliquots samples were wrapped in aluminum foil to form wafers, and stacked in quartz vials with the international standard Brione muscovite (18.7 ± 0.09 Ma [*Hall et al.*, 1984]). The vial was 40 mm in length with an inner diameter of 6.5 mm, and the position for every sample was recorded as the distance from the bottom of the vial. Then the vials were sealed in vacuo and put in a quartz canister. The canister was wrapped with cadmium foil (0.5 mm in thickness) for shielding slow neutrons in order to prevent interface reactions during the irradiation.

[21] Neutron irradiation was carried out in position H8 of 49–2 Nuclear Reactor (49–2 NR), Beijing (China), with a flux of ~6.5×10^{12} n $(cm^2\ s)^{-1}$ for 24 h, yielding J values of ~0.00499. The H8 position lies in the core of the reactor and receives flux from all directions. Specimens were rotated during the fast neutron irradiation to get homogeneously distributed neutrons. Six to eight replicate analyses of the monitors from each vial were conducted to constrain the vertical neutron fluence

gradient to within ±0.7%. This additional uncertainty was propagated into the plateau and inverse isochron ages. External uncertainties arising from the decay constants and primary K-Ar standards were not propagated. Errors are reported at the 2σ confidence level.

3.2.2. The $^{40}Ar/^{39}Ar$ Analyses

[22] The irradiated samples were transferred into a high-vacuum "Christmas tree." Following a 24 h bake at 250°C, the sample wafer was dropped into a Ta tube resting in the Ta crucible of an automated double-vacuum resistance furnace and heated at 600°C for 30 min in order to remove the effects of low-temperature alteration. Total fusion and step heating were carried out as follows: 1500°C held for 10 min for total fusion; the step heating was schemed from 700°C or 750°C to 1400 or 1500°C at a pace of 40°C or 50°C; each step took 10 min. The heating scheme is controlled by a programmed thyristor and the temperature is measured and fed back through a thermocouple which is about 1 mm under the tantalum crucial of the furnace. The extracted gas was purified by two SAES getters (NP10) for 8 to 20 min according to the volume of the release; one Zr-Al getter was operated at 80°C in order to eliminate H_2 whereas the other getter was set at 400°C to remove the active gases such as N_2, O_2 and CO_2.

[23] Isotopic measurements were made on the MM5400 mass spectrometer at IGGCAS. The procedure for $^{40}Ar/^{39}Ar$ analyses follows *Wang et al.* [2006b]. System blanks at 1500°C determined several times each day prior to degassing the samples were typically 3×10^{-16} moles of ^{40}Ar and 9×10^{-19} moles of ^{36}Ar in nearly atmospheric ratios, less than 1/200 of magnitude of sample signals. For step heating, the blanks were subtracted from sample measurements at various temperatures by interpolating the curve which was determined by a series of measured blanks.

[24] The ion currents were measured in order of ^{40}Ar, ^{39}Ar, ^{38}Ar, ^{37}Ar and ^{36}Ar, and involved eight cycles. For each peak and baseline measurement, the ion beam of ^{40}Ar, ^{39}Ar, ^{38}Ar, ^{37}Ar was integrated for 10 s, ^{36}Ar for 30 s and 4 s for baselines. Baseline measurements were basically taken at a half mass unit away from the peaks, except between ^{39}Ar and ^{40}Ar where the baseline was set at 39.3. Isotope ratios were extrapolated to zero time by the least squares regression from eight cycle measurements. Usually the "memory effect" of the instrument was negligible; the variation of $^{40}Ar/^{39}Ar$ was less than 1% in one run and the analytic error was less than 0.1%. K_2SO_4 and CaF_2 crystals were fused to calculate Ca and K correction factors: $[^{36}Ar/^{37}Ar]_{Ca} = 0.000278 \pm 0.0000142$, $[^{39}Ar/^{37}Ar]_{Ca} = 0.000852 \pm 0.0000281$, $[^{40}Ar/^{39}Ar]_{K} = 0.001182 \pm 0.000125$. Ages were calculated using the decay constant listed by *Steiger and Jäger* [1977] and all errors were quoted at the 2σ level. Mass discrimination was monitored using an online air pipette from which multiple measurements were made before and after each experiment, the mean over this period was 0.99978 ± 0.00024 per amu and the uncertainty of this value was propagated into all age calculations.

[25] Plateau ages were determined from three or more contiguous steps, comprising >50% of the ^{39}Ar released, revealing concordant ages at the 95% confidence level. The uncertainties in plateau ages reflect multiplication by the MSWD and were obtained by standard weighting of errors for individual steps according the variance [*Taylor*, 1997]. Thus, more precise determinations were given greater weight than those of lower precision and the overall uncertainty about the mean value may be greatly reduced. Because no assumption was made regarding the trapped component, the preferred ages are isochrones, calculated from the results of plateau steps using the *York* regression algorithm [*York*, 1968].

[26] Uncertainties on all data reported herein are at the 95% confidence level. Where data from the literature are discussed that were originally reported at the 68% confidence level, the uncertainties are doubled for consistency. The data herein were processed using ArArCALC [*Koppers*, 2002].

4. Results

4.1. Major and Trace Elements and Sr and Nd Isotopes

[27] The geochemical and Sr, Nd isotopic compositions of studied samples are shown in Table 1. The basalt and basaltic samples are in a limited range from 45.47 to 50.77 wt % of SiO_2, and in ranges of Al_2O_3 of 16.59–18.46 wt % and TiO_2 of 0.63–0.80 wt %. They have high total Fe abundance of 7.93–9.00 wt %, but moderate MgO of 2.88–6.03 wt %. High CaO concentrations (8.24–11.90 wt %) were determined. Medium to high LOI (3.22–8.27) suggests that the samples were heavily altered. Chondrite-normalized REE shows enrichment in light REE and depletion in heavy

Table 2. Summary of $^{40}Ar/^{39}Ar$ Analysis Results

Sample	Rock	Dating	Plateau Age (Ma)	Inverse Isochron Age (Ma)	Integrated Age (Ma)	K/Ca[a]	$^{40}Ar/^{36}Ar$ Initials
05121804	andesite	groundmass	46.30 ± 0.75	44.20 ± 1.56	44.81 ± 2.26	0.055	303.0 ± 3.5
05121903	mafic dike	groundmass	46.34 ± 0.77	43.89 ± 1.54	67.29 ± 1.47	0.066	304.0 ± 4.0
05121908	mafic dike	groundmass	45.43 ± 0.43	44.65 ± 0.85	42.25 ± 1.95	0.067	303.0 ± 6.4
05122401	diorite	K-feldspar	44.12 ± 0.60	44.02 ± 1.36	44.23 ± 0.67	0.277	295.7 ± 2.7
05122402	basalt	groundmass	48.27 ± 1.21	45.77 ± 1.68	50.38 ± 1.15	0.166	304.7 ± 3.3
05122408	mafic dike	groundmass	46.59 ± 0.38	44.63 ± 1.13	50.51 ± 0.56	0.097	319.0 ± 11.8
05122602	granodiorite	K-feldspar	44.28 ± 0.21	44.46 ± 0.27	43.84 ± 0.33	7.051	290.7 ± 4.8
05122605	propylite	groundmass	46.51 ± 0.66	44.78 ± 0.55	47.66 ± 0.45	12.88	313.9 ± 4.2

[a] $K/Ca = [^{39}Ar_K/^{37}Ar_{Ca}] \times 0.562$ [*Wang et al.*, 2006b].

REE. The initial $^{87}Sr/^{86}Sr$ and $^{143}Nd/^{144}Nd$ ratios display only limited variation of 0.703342–0.703877, and 0.512858–0.512956.

[28] The granodiorite sample has SiO_2 content of 62.28 wt %, whereas the diorite is relatively primitive as shown by the SiO_2 content of 51.01 wt %. The primitiveness of the diorite is also indicated by MgO content which is 4.00 wt %. High Al_2O_3 of 19.01 wt % suggests high plagioclase content in the diorite sample. Na_2O of 4.97 wt % and K_2O of 1.12 wt % imply that alkali feldspar in diorite is primitive as well. Samples from granodiorite and diorite have slightly higher REE contents. They display identical initial $^{87}Sr/^{86}Sr$ and $^{143}Nd/^{144}Nd$ ratios to those of basalts and basaltic andesites and mafic dikes.

[29] It is worth noting sample 05122605 which is distinct from the others studied. The low SiO_2 (48.75 wt %), MgO (3.72 wt %), CaO (2.38 wt %) and high K_2O (3.23 wt %), Al_2O_3 (24.03 wt %), total Fe (11.95 wt %) in this sample suggest it underwent metasomatic processes (Table 1). In thin section it displays a blastoporphyritic texture with main minerals including adularia, plagioclase, quartz and secondary minerals. The plagioclase is classified as labradorite by electronic probe analyses with composition of $Ab_{45-43}An_{55-57}$. The presence of adularia suggests the sample experienced strong low-temperature metasomatism. From this evidence the protolith of this propylite was most likely basaltic andesite.

4.2. The $^{40}Ar/^{39}Ar$ Analysis Results

[30] $^{40}Ar/^{39}Ar$ analysis results are presented in Table A1, and a brief summary is shown in Table 2. Age spectra and inverse isochrones are illustrated in Figure 4.

[31] All of the samples present well-resolved plateaus comprising 70%–100% of the total $^{39}Ar_K$ released. However, some of the age spectra are complicated and may warrant further discussion. When closely examining the age plateaus, evidence of minor alteration and recoil effects can be identified, such as increased $^{38}Ar_{Cl}$, high apparent ages (AP), distinct plateau and isochron ages, and differences between TF ages (TF) and plateau ages (PL ages) (Figure 3 and Tables 2 and A1). Except two K-feldspar samples presenting consistent plateau and inverse isochron ages and initial $^{40}Ar/^{36}Ar$ ratios ($(^{40}Ar/^{36}Ar)_0$) indistinguishable from the atmospheric value (295.5), all the groundmass samples show an excess Ar component indicated by the initial $(^{40}Ar/^{36}Ar)_0$ values (Table 2 and Figure 4). Erroneously old ages in low-temperature steps (700–950°C) for sample 05121903 and 05122408 account for 18% and 30% of the total released ^{39}Ar, respectively. The low-temperature discordant sections start at high apparent ages that monotonically decrease toward the age plateau (Figure 4). This observation can be explained by the recoil of $^{39}Ar_K$ (increasing the apparent ages) in combination with the preferential degassing of alteration phases (increasing the atmospheric component) that are located interstitially and on the surface of plagioclase or clinopyroxene in the groundmass [*Lo et al.*, 1994; *Koppers et al.*, 2000; *Koppers and Staudigel*, 2003]. An alternative explanation for this phenomenon is the occurrence of excess Ar due to alteration or the presence of volatiles at low temperature within samples. These possibilities are discussed in section 5.3.

[32] Excess Ar is detected in the high-temperature steps of six basalt and basaltic andesite samples as indicated by the initial $(^{40}Ar/^{36}Ar)_0$ ratios of 303–320 (Figure 4 and Table 2). Therefore, the isochron ages is considered to be more accurate for these volcanic groundmass samples.

[33] In contrast, two K-feldspar samples (05122602, 05122401), yielding flat age spectra accounting for 96% and 100% of released ^{39}Ar, respectively, do not exhibit excess Ar component as shown by initial

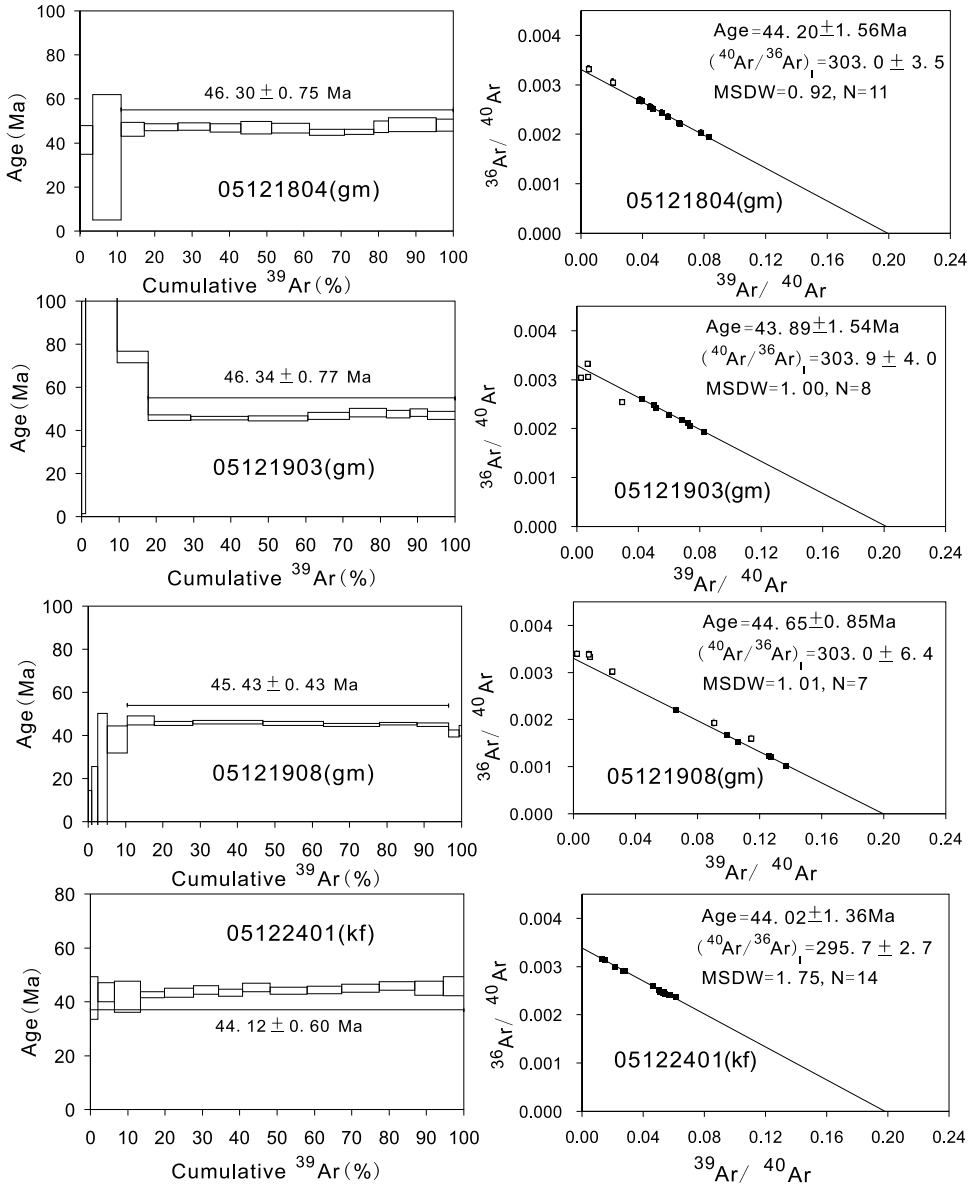

Figure 4. The $^{40}Ar/^{39}Ar$ age spectra and inverse isochron diagram. The solid squares denote the steps used for calculating the isochrons.

$(^{40}Ar/^{36}Ar)_0$ ratios of 290.7 ± 4.8 and 295.7 ± 2.7, respectively (Figure 4 and Table 2).

5. Discussion

5.1. Geochemical Affinity of the Rocks

[34] Due to their nonsusceptibility to fractionation and crystallization processes, the initial Sr and Nd isotopic compositions can be used as indicators of the source of the igneous rocks. The diorite and granodiorite have almost identical initial $^{87}Sr/^{86}Sr$ (0.703342–0.703877) and $^{143}Nd/^{144}Nd$ (0.512858–0.512956) ratios to those of the basalt, mafic dike and andesite, indicating they were derived from a common mantle source (Figure 5). The ε_{Nd}(45 Ma) values (having been corrected back to 45 Ma) of all samples are in a range from +5.4 to +7.3, strongly suggesting that they originated from a depleted mantle source similar to the DM member (Figure 5). In Figure 6, the major and trace elements from all types of rocks form uniform evolution trends: SiO_2 decreases with the increasing of MgO; FeO and Al_2O_3 increase with increasing of MgO; trace elements of V and Co increase with increasing of MgO. These granitoids plot along a same evolution trend as basalts and mafic dikes, implying that they were the products of crystal fractionation of a same parental melt as the mafic rocks.

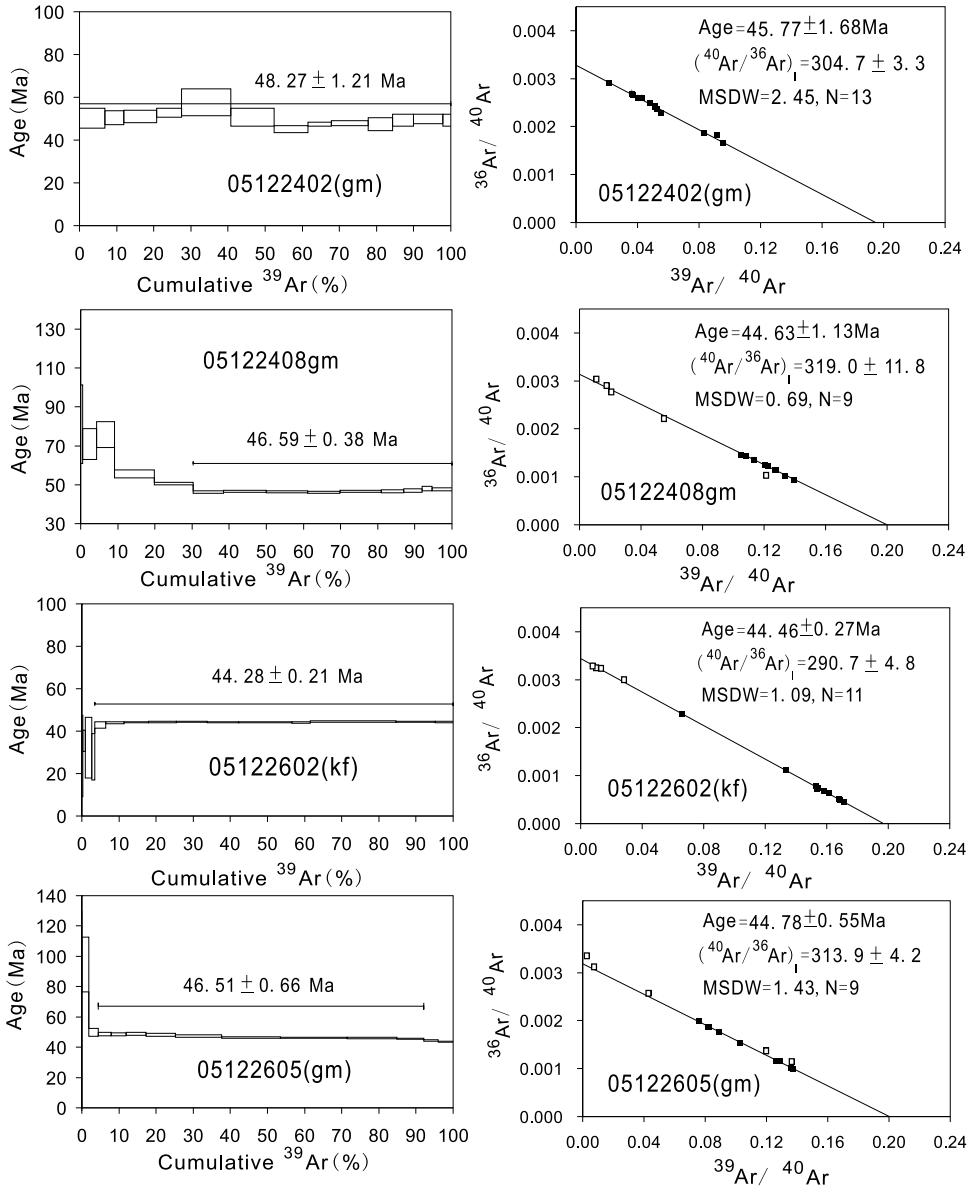

Figure 4. (continued)

[35] The incompatible element contents of sample 05122602 (granodiorite) are more typical of crustal-derived melts (Table 1) and, therefore, the possibility remains that this granodiorite was contaminated during transport through the continental crust. However, the low initial $^{87}Sr/^{86}Sr$ ratios and high ε_{Nd}(45 Ma) values suggest that the parental melts of granodiorite did not assimilate crustal materials and maintained closed system crystal fractionation during magma ascent.

[36] The chemical similarity of fifteen rare earth elements make them behave similarly during geological processes, and subtle differences in their abundance can be taken as an indicator of fractionation. All the samples in this study show similar enrichment or depletion patterns (Figure 7), but different absolute concentrations (Figure 7 and Table 1). This supports the supposition that all originated from the same source but experienced different fractionation processes. The negative Eu anomaly for sample 05122602 (Figure 7 and Table 1) indicates that this granodiorite experienced feldspar crystallization process within the crustal magma chamber.

[37] Therefore, the geochemical evidence suggests that the different igneous rocks on the Barton and Weaver peninsulas originated from a common depleted mantle source, suggesting they share a common genesis.

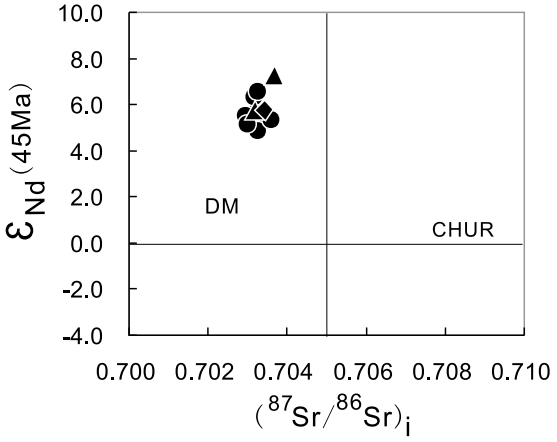

Figure 5. Diagram of ε_{Nd} (45 Ma) versus $(^{87}Sr/^{86}Sr)_i$ for the samples from Barton and Weaver peninsulas. Solid circle denotes volcanic rocks, whereas solid triangle and diamond denote the granitoids and propylite, respectively.

5.2. Alteration and Recoil Effects

[38] Such processes may result in the transformation of primary magmatic minerals, such as olivine, into hydrated secondary minerals, devitrification of glass in the interstitial spaces, and deposition of alteration products (i.e., clay, zeolites, phosphates and carbonates) in veins, cracks and vesicles. These secondary minerals often reside in small domains, prone to $^{39}Ar_K$ or $^{37}Ar_{Ca}$ recoil effects [*Fleck et al.*, 1977; *Roddick*, 1978; *Baksi*, 1974; *Lo et al.*, 1994; *Koppers et al.*, 2000]. The gain or loss of Ar, K and/or Ca during the formation of secondary minerals during alteration has a deleterious effect on the accuracy of $^{40}Ar/^{39}Ar$ ages. These observations can be reflected by the TF ages (integrated ages) such that too low or high a TF age, relative to the plateau age, is explained by the loss of $^{40}Ar^*$ due to alteration [*Fleck et al.*, 1977; *Roddick*, 1978] or by the recoil loss of $^{39}Ar_K$. In Figure 8, the TF ages of samples (assuming they formed at same time) increase with increasing LOI values, indicating that the $^{40}Ar/^{39}Ar$ analysis results were affected by the formation of alteration products or by recoil effects.

[39] Recoil effects may cause the loss and redistribution of the $^{39}Ar_K$ and $^{37}Ar_{Ca}$ when the fine-grained altered groundmass basaltic samples are irradiated [e.g., *Turner and Cadogan*, 1974; *Fleck et al.*, 1977; *Roddick*, 1978; *Pringle*, 1993; *Koppers et al.*, 2000]. This can be detected by discordance between the preirradiation and postirradiation K/Ca ratios [*Koppers et al.*, 2000]. For example, if the bulk K/Ca ratios measured during $^{40}Ar/^{39}Ar$ analyses are lower than the K/Ca ratios measured before irradiation, the groundmass samples have lost $^{39}Ar_K$ preferentially over $^{37}Ar_{Ca}$ during sample irradiation

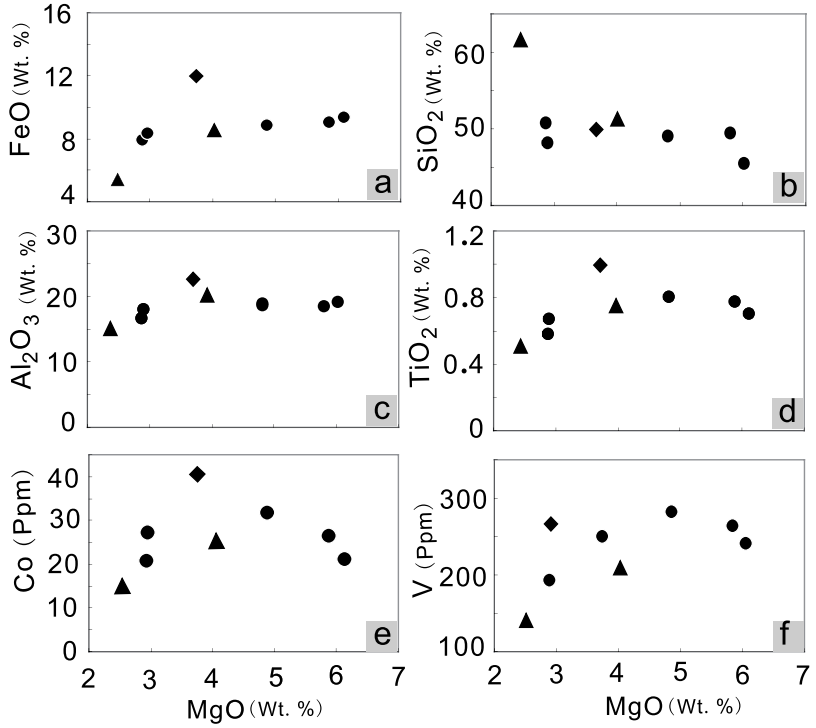

Figure 6. Plots of various oxides of FeO, Al_2O_3, SiO_2, TiO_2, and trace elements of Co and V versus MgO for all studied samples. Symbols are the same as in Figure 5.

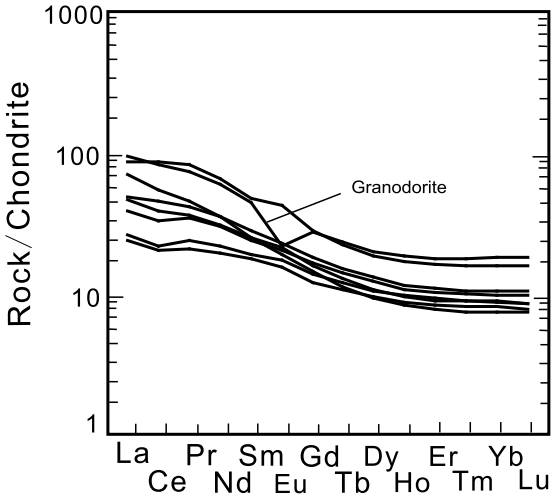

Figure 7. Chondrite-normalized REE patterns. The chondrite values are from *Sun and McDonough* [1989].

and bake-out. Therefore, the discordance in K/Ca ratios could be a useful measure of $^{39}Ar_K$ recoil in groundmass alteration minerals.

[40] Figure 9a displays the discordance between the bulk K/Ca ratios from $^{40}Ar/^{39}Ar$ analyses and K/Ca ratios determined by XRF of five basaltic groundmass samples. It is evident that most groundmass samples were impacted by $^{39}Ar_K$ recoil effects, except sample 05122402 which lost $^{37}Ar_{Ca}$ preferentially. Sample 05122502 has the highest CaO content (11.9 wt %, Table 1) which may enhance the recoil effects of $^{37}Ar_{Ca}$. Recoil effects of $^{39}Ar_K$ usually yield high apparent ages at low temperatures that monotonically decrease toward the age plateau. Samples 05122408 and 05121903 show such characteristics in their age spectra (Figure 4), indicating recoil loss of $^{39}Ar_K$

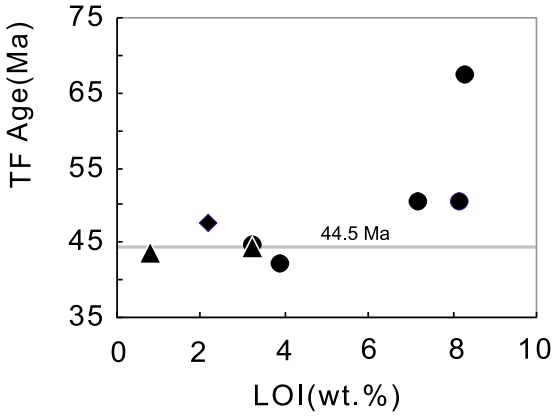

Figure 8. Relationship between LOI values and TF ages. The positive correlation indicates that the causes of the difference between TF and PL ages (such as loss of $^{40}Ar^*$ and recoil of $^{39}Ar_K$) are related to alteration processes. Symbols are the same as in Figure 5.

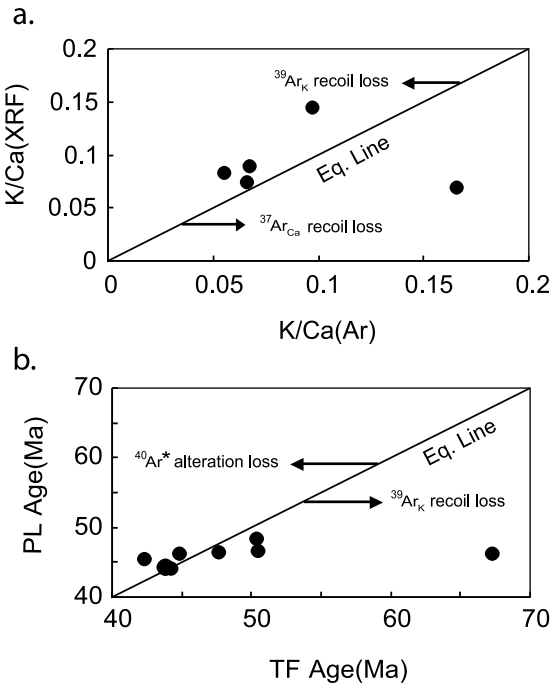

Figure 9. (a) Discordance between the bulk K/Ca ratios from $^{40}Ar/^{39}Ar$ analyses and K/Ca ratios determined by XRF of five basaltic groundmass samples. The rightward and leftward deviations from the equilibrium line reflect the $^{39}Ar_K$ and $^{37}Ar_{Ca}$ recoil losses, respectively. (b) TF age versus PL age plot. The rightward and leftward deviations from the equilibrium line suggest the $^{40}Ar^*$ loss from alteration and $^{39}Ar_K$ recoil loss, respectively. Symbols are the same as in Figure 5.

during the low-temperature steps. In contrast, at intermediate- and high-temperature steps, these two samples exhibit flat age plateaus, implying the recoil loss of $^{39}Ar_K$ is negligible. Recoil loss of $^{37}Ar_{Ca}$ indirectly causes higher $^{36}Ar/^{40}Ar$ and $^{39}Ar/^{40}Ar$ ratios as a result of overcorrecting for interference, leading to high apparent ages. For this reason, the ages (including plateau age 48.3 ± 1.2 Ma and inverse isochron age 45.8 ± 1.7 Ma) of sample 05122402 may be overestimated slightly compared with other samples. These observations are consistent with the previous studies by *Koppers et al.* [2000] who noted that for K/Ca ratios lower than 0.2 the recoil effects in altered basaltic groundmass samples will significantly increase. The K/Ca ratio of more than half of the sample in this study is less than 0.2 (Table 2).

[41] The observations above can be confirmed by noting the discordance between the total fusion age (TF age) and the plateau age (PL age). The difference between TF age and PL age suggests $^{40}Ar^*$ loss by alteration and $^{39}Ar_K$ loss by recoil effects. Most samples show lower TF ages than plateau ages

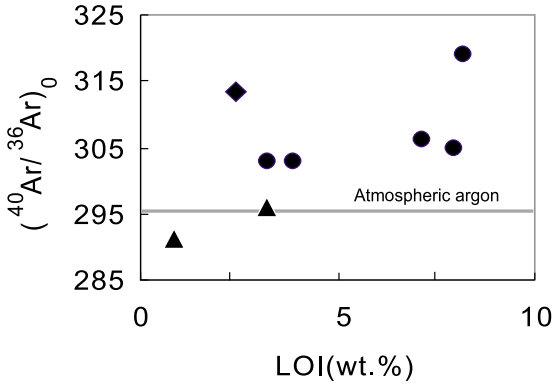

Figure 10. Plot of $(^{40}Ar/^{36}Ar)_0$ versus LOI values. Positive correlation implies a relationship of Ar initial ratios with alteration. Symbols are the same as in Figure 5.

(Figure 9b), indicating recoil loss of $^{39}Ar_K$ is the dominant cause for the discordance in TF ages.

5.3. Excess Ar

[42] It is long observed that excess Ar resides within the volcanic rocks of the South Shetland Islands [*Dupre*, 1982; *Gracanin*, 1983; *Willan and Kelley*, 1999], although the groundmass samples of basalts usually do not contain nonequilibrated phenocrysts, xenocrysts or xenoliths that introduce excess Ar or inherited Ar signatures [*McDougall and Harrison*, 1999; *Singer and Pringle*, 1996; *Singer et al.*, 1998; *Koppers et al.*, 2000; *Wang et al.*, 2006a]. In this study the $(^{40}Ar/^{36}Ar)_0$ ratios vary from 303 to 320 indicating manifest excess Ar components within these volcanic groundmass samples (Table 2 and Figure 3).

[43] Excess Ar presents in high-temperature plateau steps (Figure 3), indicating that it was tightly held in plagioclase and clinopyroxene where alteration is volumetrically less important. When *Willan and Kelley* [1999] studied plagioclase from mafic dikes in the South Shetland Islands, they attributed the excess Ar released at high temperatures to a primary component in the melt, trapped during emplacement and cooling. This interpretation confirmed previous observation of saddle-shaped step-heating patterns in $^{40}Ar/^{39}Ar$ age spectra from South Shetland Island samples [*Dupre*, 1982; *Gracanin*, 1983]. However, the relationship between LOI values and $(^{40}Ar/^{36}Ar)_0$ implies that alteration may be the source of excess Ar in our case (Figure 10). With increasing degree of alteration (indicated by LOI values), the excess component in initial Ar increases (Figure 10). From the discussion above we know that these rocks, including the granodiorite and diorite, originated from the same source at the same time and that they should have the same initial Ar composition. There are two mechanisms that may change the initial Ar composition: (1) it may be altered in the melts during ascent by exchanging Ar with the surrounding crust if the Ar composition in the crust is different from the melts or (2) it may be modified by postdepositional alteration processes in the subaerial setting. The initial Ar of two K-feldspars (Figure 4) are indistinguishable from atmosphere (295) and as phenocrysts, K-feldspars crystallized and equilibrated with the crust surrounding the magma chambers. This suggests that the crust in the studied region did not contain an excess Ar component and that it is not possible that the excess Ar originates from process 1. Low K_2O volcanic rocks are highly susceptible to fractionation of Ar isotopes and K mobility during low-temperature alteration and hydration [*Baksi*, 1974; *Lo et al.*, 1994; *Singer et al.*, 1998]. In contrast, high K contents make K-feldspar crystals far less susceptible to alteration processes and keep the same initial Ar with the melts. Therefore, we conclude the variation observed in the initial Ar is a result of secondary alteration processes.

[44] The mechanism of excess Ar incorporation during alteration as evidenced at the high-temperature plateaus is not well known. As shown in Figure 11, the low-temperature steps of 05121903 and 05122408 are characterized by increasing $^{38}Ar(Cl)/^{39}Ar(K)$ values with increasing of apparent ages, suggesting incorporation of Cl-related excess Ar, or recoil loss of $^{39}Ar_K$ or a combination of both. However, these trends are not noted in the high-temperature steps where the excess Ar resided. This ma y suggest that the recoil loss of $^{39}Ar_K$ or incorporation of Cl-related excess Ar impacted mainly the outer portion of the sample grains (i.e., the altered regions with secondary minerals in veins, cracks and vesicles) and played a less important role in the inner portion of the sample grains. This implies that the excess Ar observed in the high-temperature steps may relate to recoil effect but not to the chlorine fluids hydration alteration processes. Recoil effects could cause the redistribution of Ar within groundmass samples such that it may appear to reflect excess Ar.

5.4. Validity of the Ages

[45] Because not all of the secondary minerals, such as sericite and chlorite, will be easily removed by wet-chemical cleaning methods as some might be protected within the interiors of the groundmass minerals, they will likely affect the dating. The argon distribution patterns, presenting as flat age spectra,

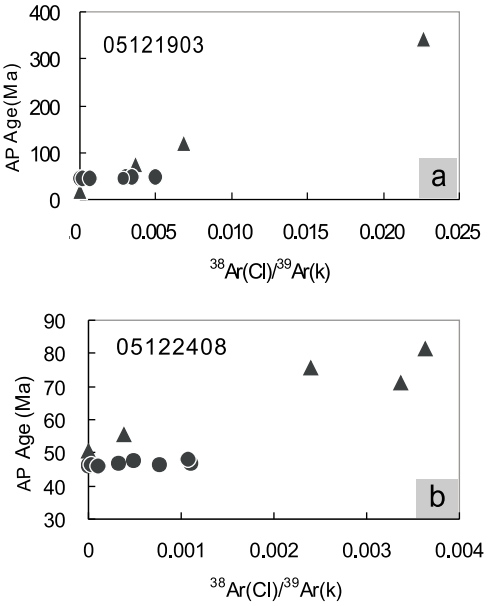

Figure 11. Relationship of $^{38}Ar(Cl)/^{39}Ar(k)$ values and AP ages of samples 05121903 and 05122605. The solid triangles denote low-temperature steps (700–950°C).

suggest the secondary minerals pose minor impact on the ages, because the secondary minerals degassing at low temperatures would have produced low apparent ages. There are four possibilities for this:

[46] 1. The alteration was thorough and complete through the core of all minerals, and more importantly, the alteration event(s) must span a short duration in order to give consistent ages at all temperature steps in experiment. This inference is not consistent with the section observation discussed above and the $^{40}Ar/^{39}Ar$ analysis data (Table A1). The $^{40}Ar/^{39}Ar$ analysis data show that the $^{40}Ar^*$ (radiogenic argon) release during step-heating experiment predominately at high-temperature steps (>1000°C), suggesting the secondary minerals are not the dominant phase in the mineral cores.

[47] 2. The hydrothermal type of alteration is of autometasomatism without change of chemistry within the rocks, therefore being of the same ages, as suggested by *Kraus* [2005]. The addition of K and Ar brought by hydrothermal fluids into the rocks may change the chemical composition.

[48] 3. The most secondary products were eliminated by preliminary treatments, so that the remnant secondary minerals is too few to affect age spectra. The amount of the alteration product can be reduced significantly by wet-chemical processing and manually picking, and more importantly, among the most secondary minerals, the sericite is the only one contains potassium.

[49] 4. The alteration event took place rapidly after the rocks formed around 44.5 Ma, or the lagging time between them was unmeasurable radiometrically. The coeval age produced by propylite sample (05122605), a typical hydrothermal alteration product, strongly suggests that the hydrothermal alteration occurred rapidly after the rocks formed, therefore being of the same ages.

[50] It seems that there are two types of alteration in these samples. The major alteration comes from hydrothermal metasomatism occurred rapidly after the rocks formed, producing the most secondary minerals and propylitic lithology. They do not affect the dating results, because of being the same ages. The minor alteration is the weathering afterward, it imposes limited impact on age spectra at the low temperatures in step-heating experiments after sample processing, as showed by sample 05121908.

[51] The additional occurrence of epidote-clinozoisite together with albite and quartz in dike samples may indicates lower greenschist facies condition (0.4–0.8 GPa, 250–400°C). This may be interpreted with the stratigraphically much lower position of these dikes as part of the "root" of the magmatic arc, coming along with higher temperature and pressure [*Kraus*, 2005]. If it is true, we will expect some impacts on plagioclase (with closure temperature of 250–350°C) to cause radiogenic argon loss, but not on high-temperature phases such as pyroxene (closure temperature of ~650°C). This can be recognized from step-heating experiments in the form of low apparent ages from gas released in the lower temperatures [*McDougall and Harrison*, 1999]. The even distribution of radiogenic argon, as indicated by age spectra, does not reflect the expectation. The most possible interpretation is that the metamorphism was a by-product from the hydrothermal metasomatism related to the plutonism emplaced around 44.5 Ma, and the rock kept close to the argon isotopic system since then. An alternative explanation is that the high pressure protected the minerals from losing argon. Experimental evidence and geological observations indicate that argon diffusion depends not merely on temperature (and cooling rate), but also on pressure [e.g., *Carroll*, 1991; *Chen et al.*, 1995; *Kelley and Wartho*, 2000; *Maurel et al.*, 2003; J. Ying and F. Wang, unpublished data, 2009]. Under high pressure, the diffusion of argon is negligible and keeps the initial argon distribution, even at the temperature above closure temperature. This may be also the reason for excess argon take-up during hydrothermal alteration in these samples.

[52] Given the consistency of intrusive rock ages (diorite and granodiorite), the extrusive rock (basalt, andesite, mafic dikes) ages could be interpreted as regional resetting times due to intrusion of the plutons (Figure 2). However, the following lines of evidence indicate that the resetting effect was not pervasive on the South Shetland Islands and the ages obtained above are not necessarily resetting times. The first evidence comes from the flat age spectra obtained in this study and literatures [*Willan and Kelley*, 1999; *Zheng et al.*, 2003; *Kraus*, 2005; *Kamenov et al.*, 2005]. The resetting from heat event normally causes rising age spectra from the low temperature during step-heating experiment. Although in some cases the resetting could be complete throughout the mineral core and produce flat age spectra either, such as in a contact zone with pluton or within a fault zone [*Willan and Kelley*, 1999], *Zheng et al.* [1997] reported an undisturbed $^{40}Ar/^{39}Ar$ isochron age of 105.6 ± 2.1 Ma for a lava samples 500 m away from the contact of the Barnard Point pluton, suggesting that the resetting effect is not so strong to influence a wider range. The flat plateaus with the similar ages (40–50 Ma) yielded by plagioclase mineral separates suggests that regional resetting on King George Island was unlikely [*Willan and Kelley*, 1999]. Resetting of the Ar systematics in plagioclase requires temperatures over 250°C but regional metamorphism studies indicate temperatures in the 150–200°C range [*Willan and Kelley*, 1999]. Furthermore, intravolcanic sedimentary sequences in the Barton and Weaver peninsulas contain sandstone and siltstone [*Lee et al.*, 2002], indicating that these volcanic rocks were at the paleosurface when they erupted, making the impact of heating from intrusions in deep crust negligible. If the volcanics covering so vast area, compared to the relative small outcrop of plutons, were reset so thoroughly that the argon in the innermost core of the minerals (even in the pyroxene) escaped completely, the ground surface temperature should be more than 650°C. This is impossible. Finally, *Kraus* [2005] and *Kim et al.* [2000] reported late Cretaceous ages of basaltic dikes on King George Island also indicate that resetting of lavas at this locality was not pervasive. Therefore, we conclude that the ages of the volcanic rocks obtained in this study are not resetting times, but reflect the eruption dates.

5.5. Implication of the Ages

[53] The new data presented here indicate that the igneous activity forming the subaerial cover rocks on Barton and Weaver peninsulas was emplaced at 44–45 Ma, in contrast to some previous results [e.g., *Park*, 1989; *Lee et al.*, 1996; *Zheng et al.*, 2000], although the older volcanic rocks may be present at depth beneath this subaerial cover rocks [*Zheng et al.*, 2000].

[54] The previous study gave whole rock K-Ar ages of 42–45 Ma [*Park*, 1989] for the granodiorite of Barton Peninsula, and 44.3 ± 0.2 Ma was obtained in this study. Due to larger grain sizes and the different Ar degassing properties of different minerals, such a coarse-grain intrusive rock is not suitable for dating by whole rock methods, which may explain the large uncertainty on the ages given by *Park* [1989]. Previous reported ages for this pluton are two biotite K-Ar ages of 41.9 ± 0.9 Ma and 41.2 ± 0.9 Ma [*Lee et al.*, 1996], even younger than the wall volcanic rocks (44 Ma in this study). The extremely flat age spectrum of the K-feldspar, accounting for 95% of ^{39}Ar released, shows that the radiogenic $^{40}Ar^*$ is quite homogenously distributed, implying a rapid cooling rate, and an age representative of the emplacement of the pluton. The K-feldspar from the fine-grained diorite of Weaver Peninsula yielded a plateau age of 44.1 ± 0.6 Ma. The absence of an age gradient in the age spectrum, accounting for 100% of released ^{39}Ar also suggests a rapid cooling process in the crust. The age of this K-feldspar is also indicative of the timing of pluton emplacement. A previously reported whole rock $^{40}Ar/^{39}Ar$ age on this diorite was 48.4 ± 0.5 Ma [*Kim et al.*, 2000]. The widely distributed EW dikes on the Weaver Peninsula were emplaced almost coevally with the diorite as indicated by two ages (44.7 ± 0.8 Ma and 44.6 ± 1.1 Ma, on samples 05121908 and 05122408, respectively). These ages reveal that there is no distinguishable time gap between the emplacement of EW dikes and NS dikes, the latter yielding an isochron age of 43.9 ± 1.5 Ma (sample 05121903 from the Weaver Peninsula). The basaltic and andesitic lavas from the Barton and Weaver peninsulas also erupted at 44–45 Ma as evidenced by three isochron ages of 44.2 ± 1.6 Ma (05121804, basalt from Barton Peninsula), 45.8 ± 1.7 Ma (05122402gm, basaltic andesite from Weaver Peninsula) and 44.8 ± 0.6 Ma (05122605, altered andesite from Barton Peninsula).

[55] Deep hydrothermal fluids related to the magmatism are prevalent in the crust in island arc settings and may cause low-temperature metasomatism. Sample 05122605, a hydrothermally altered andesite (propylite), could reveal the timing of

metasomatism. This sample exhibits a flat age spectrum with a plateau accounting for >80% of the released $^{39}Ar_K$ and yields an age of 46.5 ± 0.7 Ma (Figure 4 and Table 2). Nine steps form a well correlated isochron, yielding an inverse isochron age of 44.8 ± 0.6 Ma with an $[^{40}Ar/^{36}Ar]_0$ value of 313.9 ± 4.2, distinct from that of atmosphere. The high average K/Ca value (~12 (Table A1)), calculated from $^{39}Ar[k]/^{37}Ar[Ca]$ ratios, suggests that the main phase which dominated the degassing pattern of Ar, was adularia as discussed above. The low LOI value (2.16 wt % (Table 1)) indicates that the subaerial alteration had a relatively minor effect. This is reflected by the stable Ar release pattern at low- and high-temperature steps in the age spectrum (Figure 4). A flat age spectrum and an isochron age identical to that of other lavas in this area suggest that propylitic metasomatism is pervasive and rapid following the eruption of lavas. Pervasive metasomatism either ceased or moderated to a degree that further redistribution of Ar within minerals did not occur.

5.6. Significance for the Tertiary Geodynamic Setting of the Antarctic Peninsula

[56] The magmatism on the Barton and Weaver peninsulas must be related to the subduction history of the southeastern Pacific Ocean floor beneath the Antarctic continent. Lavas, plutons and mafic dike swarms on the Barton and Weaver peninsulas originated from a common depleted mantle source and formed approximately at same time (~44.5 Ma) suggesting that the major igneous activity on Barton and Weaver peninsulas was constrained in a short period of 44–45 Ma. Is it a particular pulse of magmatism on these two peninsulas, or a common feature in the South Shetland Islands? This can be better understood within a panorama of igneous activity on the archipelago under plate tectonics.

5.6.1. Giant Igneous Event in the South Shetland Islands

[57] South Shetland arc rocks are exposed for 300 km parallel to the continental margin, and contain a relatively long record of arc igneous activity spanning early Cretaceous (~140 Ma) [*Pankhurst and Smellie*, 1983] or mid-Cretaceous (~115 Ma) [*Willan and Kelley*, 1999] to middle Miocene times [*Pankhurst and Smellie*, 1983; *Smellie et al.*, 1984; *Birkenmajer*, 1994; *Willan and Kelley*, 1999]. Previous radiometric dating results in the South Shetland Islands suggest that igneous activity migrated from SW to NE along the arc during Mesozoic-Tertiary times [*Pankhurst and Smellie*, 1983; *Birkenmajer et al.*, 1986]. *Birkenmajer* [1994] related this trend to counter clockwise rotation of the Antarctic plate over a stationary hot spot, while *Barker* [1982] attributed it to the cessation of calc-alkaline magmatism with consumption of Aluk Ridge, although it seems as though cessation took place as the ridge crest approached, up to 50 Ma prior to collision, i.e., when young oceanic crust was being subducted. This effect was ascribed to dehydration of younger, more buoyant oceanic crust at shallow depths where melting could not occur [*Delong et al.*, 1979; *Pankhurst and Smellie*, 1983].

[58] The newest compilation of ages (Table A2 and Figure 12) including recently published data and this study indicates that the mid-Eocene (40–50 Ma) igneous rocks are also widespread on the Livingston Island, the SW end of the South Shetland Islands [*Smellie et al.*, 1996; *Kamenov*, 1997; *Willan and Kelley*, 1999; *Zheng et al.*, 2003; *Kraus*, 2005; *Kamenov et al.*, 2005]. Figure 12a shows that Livingston Island is characterized with a major episode of igneous activity from 50 to 40 Ma, peaking at ~45 Ma, although it started ~140 Ma ago. Of all the ages, the Cretaceous ages on Livingston Island are mainly contributed by K-Ar ages from the early publications [*Pankhurst and Smellie*, 1983; *Smellie et al.*, 1984; *Birkenmajer et al.*, 1986], which were partly reevaluated by *Willan and Kelley* [1999] and *Kraus* [2005] and found that some Cretaceous ages are unreliable due to either Ar and K loss, and excess argon presence [*Willan and Kelley*, 1999; *Kraus*, 2005]. Although we still include these ages in compilation, we should notice that the igneous activity in Livingston was not as strong in Cretaceous times as claimed. Therefore, these evaluation studies [*Willan and Kelley*, 1999; *Kraus*, 2005] enhance our contention that major igneous activity on Livingston Island is around 45 Ma, and attenuated apparently after 40 Ma.

[59] To the NE, the King George Island has a similar distribution pattern of ages in the probability diagram (Figure 12b). The peak probability of ages around 45 Ma indicates that the igneous activity culminated synchronously with the Livingston Island at this time.

[60] Thus it can be concluded that Cretaceous to Tertiary magmatic activity occurred throughout the South Shetland Islands. Put all the above data together (166 ages), the relative probability diagram indicate that 50–40 Ma is the most important

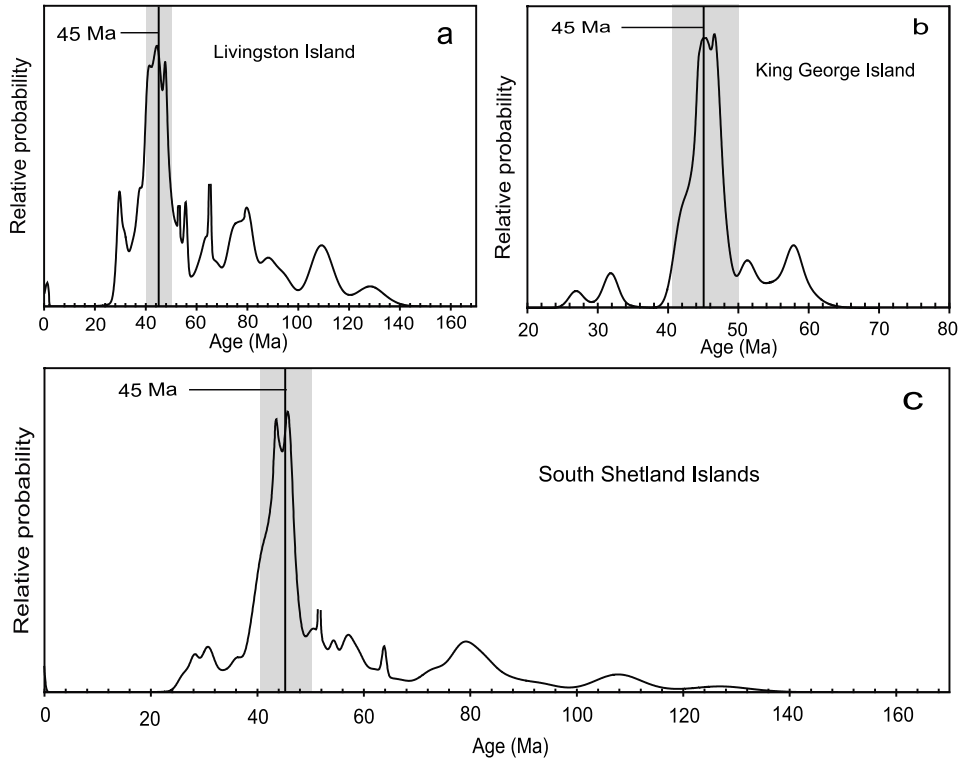

Figure 12. Age probability diagrams for the Cretaceous to Tertiary igneous rocks in (a) Livingston Island, (b) King George Island, and (c) the South Shetland Islands as a whole (n = 166), showing that 50–40 Ma is an important period of igneous activity in the South Shetland Islands. Data are summarized from *Pankhurst and Smellie* [1983], *Smellie et al.* [1984], *Birkenmajer et al.* [1986], *Smellie et al.* [1996], *Kamenov* [1997], *Willan and Kelley* [1999], *Zheng et al.* [2003], *Kraus* [2005], *Kamenov et al.* [2005], and this study. Gray bars indicate time range of 50–40 Ma.

period of igneous activity, with a peak at ~45 Ma (Figure 12c). Although subduction continued until the mid-Pliocene [*Barker*, 1982], and there is sparse early magmatism on the South Shetland Islands, there is no radiometric evidence in the region for magmatism of this age related to this process.

5.6.2. Nature and Significance of the Mid-Eocene Giant Igneous Event in the South Shetland Islands

[61] The data presented above indicate that the period 50–40 Ma was a time of both intensive and extensive igneous activity on the South Shetland Islands. So what cause this giant igneous event? It has long been recognized that the igneous activity on the South Shetland Islands is related to the subduction history of Phoenix Plate beneath the Antarctic continent [*Alabaster and Storey*, 1990; *Storey and Alabaster*, 1991; *McCarron and Millar*, 1997; *Scarrow et al.*, 1998]. However, this pronounced igneous event must be detailed with a new mechanism, although the magmatism succession from Cretaceous to early Miocene reflect the continuous subduction and the sharp weakening in igneous activity since early Miocene can be explained by the subduction of young oceanic crust at a shallow depth where melting would not occur [*Delong et al.*, 1979; *Pankhurst and Smellie*, 1983].

[62] The giant igneous event is usually related to the mantle plume and thickened lithosphere delamination. Due to the relative cold setting, it is unlikely to form a mantle plume beneath the arc system. Thinning of the mantle wedge may be an automatic response to lithospheric thickening as a result from the subduction. This mechanism would bring hot asthenosphere into contact with the Moho [*Bird*, 1979], and tapped melt sources in lithosphere and lower crust. This should promote massive asthenospheric and lithospheric and crustal melting and predicts a resultant magmatism in the direction of delamination [*Turner et al.*, 1999].

[63] Geochemical and isotopic composition in this study show that different types of rock on Barton and Weaver peninsulas represent partial melts of a common depleted mantle source. Other distinct mantle sources beneath the South Shetland Islands were recognized recently [*Scarrow et al.*, 1998; *Kraus*, 2005]: a low-ε_{Nd}, garnet-bearing, lithospheric

mantle (older calc-alkaline); a high-ε_{Nd}, spinel-bearing, asthenospheric mantle (younger calc-alkaline); E-MORB-like spinel-bearing asthenosphere depleted by a previous melting event (tholeiites). Slab-derived fluids, subducted sediment, and arc crust also contributed to the magmas, and compositional trends observed in volcanic rocks could be created from the addition of a relative constant subduction component to temporally varying heterogeneous mantle sources [*Lee et al.*, 2008]. *Lee et al.*'s [2008] noted that the older volcanic rocks characterized with higher radiogenic Pb and Sr isotopes and lower $^{143}Nd/^{144}Nd$ ratios, and the younger volcanic rocks with the contrary trait imply a composition shift from a enriched mantle source to a depleted asthenospheric mantle source from 140 to 44 Ma.

[64] Temporally, this source composition changing coincided roughly with the abrupt decrease in convergence rate between Antarctica and phoenix Plates at early Eocene [*McCarron and Larter*, 1998]. This rate decreased 60% at 52 Ma from 102 mm/yr to 42 mm/yr, and to 32 mm/yr (calculate from the spreading rate of 16 mm/yr by *Barker* [1982], assuming symmetric spreading) during 50–36 Ma [*Barker*, 1982]. The convergence rate increased again to 64 mm/yr from 36 to 6 Ma [*Barker*, 1982]. On this basis it seems likely, as suggested by *Storey et al.* [1996], that such a decrease in convergence rate would have a profound effect on the stress regime of the overriding plate, enhancing slab rollback and therefore causing extension within the arc and fore-arc regions. Emplacement of mafic dike swarm, plugs, sills, and tholeiitic melts (gabbro) widespread over the South Shetland Islands, culminating around 45 Ma [*Willan and Kelley*, 1999; *Kraus*, 2005], suggests that the change in subduction parameters resulted in extension and sufficient lithospheric thinning to allow decompressive melting of the mantle wedge and more than one mantle sources to be tapped.

[65] Exhumation of the metamorphic complex on Smith Island in the southern end of the South Shetland Islands suggests an uplift of lithosphere and rapid extensional setting. The metamorphic complex consists of blueschists, paragneisses and orthogneisses [*Birkenmajer*, 1994]. It may have been formed by underplating beneath the margin of Gondwanaland before breakup, beneath a subsequently accreted terrane or beneath the Pacific margin of the Antarctic Peninsula [*Henriet et al.*, 1992]. The mineral assemblages in the blueschist suggest burial down to pressure conditions of 600–800 MPa (24–30 km depth) [*Henriet et al.*, 1992]. Uplift of this blueschists occurred at some time after 47 Ma [*Trouw et al.*, 1998]. A speculative explanation of the blueschist terrane exhumation is the collision of an active margin and a buoyant ridge, or at least a ridge with a considerable relief [*Henriet et al.*, 1992]. But normally, the amount of uplift by this isostatic adjustment is only about 1–3 km in a convergent system [*England and Molnar*, 1990], not enough to exhumate the Smith complex to a shallow depth. Therefore, the exhumation of Smith complex should result from different mechanics. Uplift of Livingston Island occurred at some time between 41 and 30 Ma, as suggested by *Willan and Kelley* [1999] account to the emplacement of the coarse-grained Barnard Point pluton followed by epithermal-textured veins associated with dikes swarm. The fast cooling of granodiorite and diorite in Barton and Weaver peninsulas, being indicated by the flat K-feldspar age spectra, suggest a rapid uplift and exhumation to depth of 3 km in this locality at 44.5 Ma (calculate under assumption of 50°C/km for thermal gradient and closure time of 150°C for the finest domain of K-feldspar [*McDougall and Harrison*, 1999]).

[66] Based on the discussion above, we propose a delamination model to explain the giant igneous event and related geological phenomena occurred during 50–40 Ma. We suppose delamination of thickened mantle wedge beneath the South Shetland Islands occurred during early to mid-Eocene times. Prior to the delamination, the driving forces from subduction and the buoyancy forces of the mantle wedge were in balance, the igneous activity was related to the subduction. Continued diving of Phoenix Plate shortened and thickened the lithosphere of the mantle wedge beneath the South Shetland Islands. The strain intensified gradually enough to have the thickened lithosphere delaminated at ~52 Ma. This led to asthenosphere upwelling, and the sudden uprising of asthenosphere baffled the subduction and caused rollback of Phoenix Plate. This caused the abrupt decrease in convergence rate during 50–30 Ma [*McCarron and Larter*, 1998; *Barker*, 1982]. Heat brought by the uprising asthenospheric mantle flow then triggered multiple mantle sources forming various types of mafic lavas and gabbro intrusions, and melting in the crust forming andesitic and dacitic lavas, and plutons ranging in composition from diorite and tonalite to granodiorite and granite [*Birkenmajer*, 1994]. With the delamination progressed, the lower hump of the previously thickened mantle wedge detached completely, the

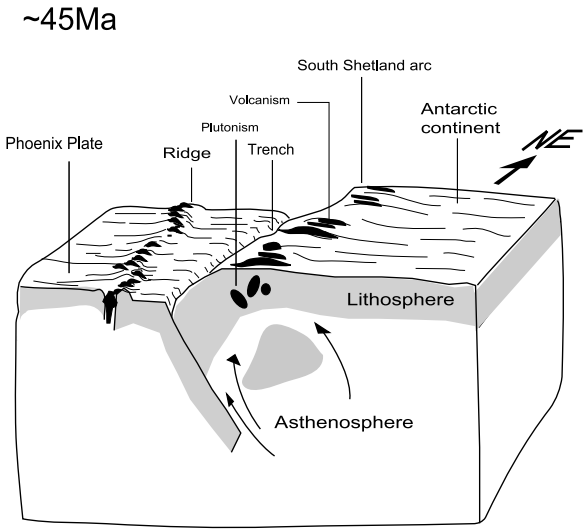

Figure 13. Speculative geodynamic scenario of South Shetland arc during Eocene. Delamination of thickened mantle wedge caused asthenospheric mantle uprising, which disturbed the subduction and resulted in an abrupt decrease in convergence rate at ~52 Ma and then triggered multiple mantle sources, causing culminating igneous activity during 50–40 Ma on the archipelago. This also resulted in an extension regime, uplift of Smith blueschist, and Livingston Island.

magmatic activity culminated during 50–40 Ma with peak at ~45 Ma. The source materials included those from depleted mantle (asthenosphere), previously metasomatized mantle, and lower crust, with different degree contribution from subducted sediments and slab-derived fluids, exhibiting heterogeneity chemically observed in the sources region. The buoyancy of uprising of asthenosphere and the rollback of subducted slab caused uplift of the Smith metamorphic complex and Livingston Island at some time after 47 Ma [*Trouw et al.*, 1998], and developed an extension regime at around during 50–40 Ma introducing feeder veins of dikes, plugs and sills. The delamination process may finished at some time during 40–30 Ma, the uprising of asthenospheric mantle flow diminished, therefore the convergence rate between Antarctica and phoenix Plates recovered gradually during 30–6 Ma [*Barker*, 1982]. But the dipped slab was at a shallower depth at this stage due to the effects of buoyancy of the mantle flow and with the approaching of the ridge crest. This caused the subduction-related magmatism lessened significantly during the late Tertiary times [*Willan and Kelley*, 1999]. This mechanism may be supported by recent seismic observation for deep high-velocity anomalies in the transition zone beneath the Antarctic Peninsula [*Sieminski et al.*, 2003].

[67] This speculative geodynamic scenario of South Shetland arc in Eocene times is simplified in Figure 13.

6. Conclusions

[68] Groundmass samples exhibit limited grain size variations, enrichment in K and equilibrium with atmospheric Ar, making them an ideal candidate for $^{40}Ar/^{39}Ar$ dating. However, a high degree of alteration compromises these advantages. Alteration-related recoil effects and excess Ar are observed in the Antarctic volcanic samples. Elaborate preparation processes, including acid leaching, acetone washing, hand picking and overnight baking yielded groundmass samples that could produce accurate age results. This suggests that the alteration effects can be eliminated or minimized to produce age plateau composed of 70%–100% of total $^{39}Ar_k$ released.

[69] Precise dating suggests that there was a giant igneous event on Barton and Weaver peninsulas at ~44.5 Ma. With the compilation including the newly published data and data in this study, we found that this event took place throughout the whole South Shetland Islands. This may modify the previous model of counter clockwise rotation of the Antarctic plate over a stationary hot spot. We check various geological events occurred during 50–40 Ma, in tectonics, geochemistry and geophysics, and frame them within a new model.

[70] We suppose delamination occurred beneath the South Shetland arc around 52 Ma responsible for the giant igneous event. The upwelling of the asthenosphere blocked the subduction of the Phoenix plate and caused a sudden decrease in the convergence rate. Then the hot asthenosphere contacted the Moho and tapped various magma sources, producing massive magmatic extrusion and intrusion along the archipelago during 50–40 Ma with a peak around 45 Ma. This model also can explain other geological phenomena occurred during 50–40 Ma: heterogeneity in the mantle source, the extension regime, the uplift of Smith blueschist and Livingston Island, the recovery of the convergence rate during 30–6 Ma, and the attenuation of the igneous activity since the early Miocene times. Seismic evidence, showing high-velocity anomalies in the transition zone beneath the Antarctic Peninsula, provides us a direct evidence for this model.

Appendix A

[71] Argon isotope analysis results are presented in Table A1. $^{36}Ar[a]$, $^{37}Ar[Ca]$, $^{38}Ar[Cl]$, $^{39}Ar[k]$,

Table A1. The $^{40}Ar/^{39}Ar$ Analysis Results[a]

Temperature (°C)	$^{36}Ar[a]$[b]	$^{37}Ar[Ca]$[b]	$^{38}Ar[Cl]$[b]	$^{39}Ar[k]$[b]	$^{40}Ar[r]$[b]	Age ± 2σ (Ma)	$^{40}Ar[r]$[b] (%)	$^{39}Ar[k]$[b] (%)	K/Ca[c] ± 2σ
				05121804, J = 0.0049360 ± 0.0000099					
700	0.000049	0.000922	0.000001	0.000092	−0.006501	−779.93 ± 43.02	−81.70	0.13	0.06 ± 0.01
780	0.000365	0.013074	0.000012	0.002448	0.011503	41.47 ± 6.49	9.64	3.35	0.11 ± 0.01
840	0.003883	0.017338	−0.000006	0.005531	0.020948	33.49 ± 28.55	1.79	7.58	0.19 ± 0.02
880	0.000316	0.009870	−0.000003	0.004473	0.023472	46.24 ± 3.15	20.06	6.13	0.26 ± 0.01
920	0.000230	0.014600	0.000001	0.006651	0.035591	47.14 ± 1.56	34.37	9.11	0.26 ± 0.02
960	0.000220	0.016819	0.000008	0.006229	0.033564	47.46 ± 1.60	34.09	8.53	0.22 ± 0.01
1000	0.000255	0.020749	0.000023	0.006075	0.032310	46.86 ± 1.86	30.03	8.32	0.17 ± 0.01
1040	0.000403	0.031787	0.000091	0.005927	0.031635	47.02 ± 2.87	20.98	8.12	0.11 ± 0.01
1080	0.000348	0.059340	0.000176	0.007445	0.039512	46.76 ± 2.27	27.77	10.20	0.07 ± 0.00
1120	0.000178	0.026106	0.000062	0.006828	0.034786	44.91 ± 1.34	39.74	9.35	0.15 ± 0.01
1160	0.000136	0.020582	0.000036	0.005780	0.029554	45.07 ± 1.14	42.40	7.92	0.16 ± 0.00
1220	0.000163	0.035121	0.000068	0.002844	0.015291	47.37 ± 2.62	24.07	3.90	0.05 ± 0.00
1300	0.000668	0.128138	0.000166	0.009346	0.051251	48.30 ± 3.09	20.61	12.80	0.04 ± 0.00
1400	0.000181	0.039616	0.000025	0.003333	0.018189	48.06 ± 2.73	25.38	4.57	0.05 ± 0.00
				05121903, J = 0.0049540 ± 0.0000099					
750	0.000107	0.001394	0.000000	0.000217	0.000413	17.00 ± 15.50	1.29	1.07	0.09 ± 0.01
810	0.000313	0.008143	0.000005	0.000698	0.009642	119.76 ± 9.91	9.43	3.45	0.05 ± 0.00
860	0.001351	0.038392	0.000023	0.001024	0.043176	342.91 ± 22.34	9.76	5.06	0.02 ± 0.00
910	0.000147	0.077957	0.000006	0.001670	0.014101	74.11 ± 2.73	24.55	8.25	0.01 ± 0.00
960	0.000068	0.022391	0.000000	0.002297	0.011939	45.97 ± 1.27	37.28	11.35	0.06 ± 0.00
1010	0.000074	0.016198	0.000001	0.003134	0.016172	45.65 ± 0.80	42.36	15.48	0.11 ± 0.00
1060	0.000104	0.017960	0.000002	0.003234	0.016644	45.52 ± 1.11	35.07	15.98	0.10 ± 0.00
1110	0.000111	0.016958	0.000007	0.002236	0.011802	46.68 ± 1.65	26.37	11.05	0.08 ± 0.00
1170	0.000126	0.019464	0.000010	0.002024	0.011073	48.35 ± 1.97	22.95	10.00	0.06 ± 0.00
1230	0.000049	0.011699	0.000004	0.001275	0.006872	47.63 ± 1.72	32.04	6.30	0.06 ± 0.00
1300	0.000045	0.009198	0.000003	0.000930	0.005083	48.33 ± 1.70	27.82	4.59	0.06 ± 0.00
1400	0.000042	0.015057	0.000004	0.001502	0.007980	46.97 ± 1.87	39.02	7.42	0.06 ± 0.00
				05121908, J = 0.0049900 ± 0.0000100					
750	0.000278	0.004222	0.000004	0.000802	−0.000300	−3.37 ± 17.72	−0.37	0.99	0.11 ± 0.01
800	0.000424	0.012339	0.000003	0.001304	0.001471	10.14 ± 15.54	1.16	1.61	0.06 ± 0.00
850	0.003229	0.038373	0.000002	0.001970	−0.006113	−28.22 ± 78.41	−0.64	2.43	0.03 ± 0.00
900	0.000535	0.058154	0.000003	0.004428	0.018915	38.14 ± 6.29	10.68	5.47	0.04 ± 0.00
950	0.000195	0.026141	0.000005	0.005843	0.030760	46.89 ± 2.08	34.81	7.21	0.13 ± 0.00
1000	0.000141	0.025101	0.000002	0.008321	0.042569	45.58 ± 0.99	50.52	10.27	0.19 ± 0.02
1050	0.000220	0.040802	0.000006	0.015196	0.078694	46.14 ± 0.79	54.71	18.76	0.21 ± 0.00
1090	0.000224	0.035982	0.000009	0.013157	0.067334	45.60 ± 0.92	50.45	16.24	0.21 ± 0.01
1130	0.000117	0.041399	0.000009	0.012148	0.061178	44.88 ± 0.64	63.95	14.99	0.17 ± 0.00
1170	0.000061	0.027891	0.000013	0.008177	0.041714	45.46 ± 0.61	69.92	10.09	0.17 ± 0.01
1230	0.000067	0.091383	0.000014	0.006884	0.034759	45.00 ± 0.89	63.70	8.50	0.04 ± 0.00
1310	0.000031	0.066781	0.000003	0.002221	0.010190	40.94 ± 1.55	52.45	2.74	0.02 ± 0.00
1400	0.000012	0.007676	0.000000	0.000568	0.002685	42.20 ± 2.39	42.78	0.70	0.04 ± 0.00

Table A1. (continued)

Temperature (°C)	^{36}Ar[a][b]	^{37}Ar[Ca][b]	^{38}Ar[Cl][b]	^{39}Ar[k][b]	^{40}Ar[r][b]	Age ± 2σ (Ma)	^{40}Ar[r][b] (%)	^{39}Ar[k][b] (%)	K/Ca[c] ± 2σ
				05122401, J = 0.0048950 ± 0.0000098					
730	0.000238	0.000703	0.000000	0.001129	0.005335	41.36 ± 7.89	7.05	2.04	0.93 ± 0.06
780	0.000258	0.002007	0.000002	0.002421	0.012048	43.52 ± 3.47	13.66	4.37	0.70 ± 0.16
860	0.000973	0.008974	0.000001	0.003895	0.018651	41.90 ± 5.74	6.09	7.03	0.25 ± 0.01
900	0.000138	0.006111	0.000001	0.003536	0.017246	42.66 ± 1.09	29.77	6.38	0.33 ± 0.01
940	0.000244	0.006077	0.000002	0.004351	0.021543	43.31 ± 1.65	23.02	7.85	0.41 ± 0.01
980	0.000186	0.004427	0.000002	0.003685	0.018711	44.40 ± 1.60	25.36	6.65	0.48 ± 0.01
1020	0.000151	0.003698	0.000000	0.003534	0.017534	43.39 ± 1.35	28.20	6.38	0.55 ± 0.02
1070	0.000185	0.004160	0.000001	0.004110	0.021292	45.28 ± 1.52	27.99	7.42	0.57 ± 0.02
1120	0.000256	0.006699	0.000003	0.005483	0.027629	44.06 ± 1.27	26.76	9.90	0.47 ± 0.01
1160	0.000219	0.006467	0.000003	0.005142	0.026120	44.42 ± 1.42	28.77	9.28	0.46 ± 0.01
1200	0.000262	0.007502	0.000001	0.005573	0.028724	45.06 ± 1.54	27.04	10.06	0.43 ± 0.01
1240	0.000257	0.006527	0.000002	0.005247	0.027566	45.92 ± 1.59	26.64	9.47	0.46 ± 0.02
1300	0.000462	0.012731	0.000003	0.004221	0.021721	44.98 ± 2.65	13.72	7.62	0.19 ± 0.00
1400	0.000425	0.012826	0.000006	0.003065	0.016064	45.81 ± 3.56	11.33	5.53	0.13 ± 0.00
				05122402, J = 0.0049960 ± 0.0000101					
750	0.000628	0.005104	0.000004	0.008402	0.047411	50.28 ± 4.60	20.35	6.81	0.95 ± 0.04
780	0.000414	0.005754	0.000005	0.006368	0.036102	50.51 ± 3.20	22.80	5.16	0.64 ± 0.02
820	0.000494	0.014936	0.000001	0.010896	0.062454	51.06 ± 2.97	29.97	8.83	0.42 ± 0.04
860	0.000341	0.011907	0.000001	0.008192	0.048642	52.87 ± 2.11	32.53	6.64	0.39 ± 0.02
900	0.002261	0.041406	0.000004	0.016415	0.106382	57.62 ± 6.27	13.73	13.30	0.23 ± 0.01
940	0.001054	0.094477	0.000001	0.014388	0.081889	50.70 ± 4.22	20.81	11.66	0.08 ± 0.00
980	0.000225	0.067994	0.000007	0.011257	0.056932	45.12 ± 1.56	46.13	9.12	0.09 ± 0.00
1030	0.000138	0.010587	0.000000	0.007866	0.041865	47.46 ± 0.93	50.60	6.37	0.43 ± 0.01
1080	0.000276	0.015536	0.000007	0.012229	0.065663	47.87 ± 1.18	44.64	9.91	0.45 ± 0.02
1140	0.000493	0.018305	0.000018	0.008101	0.043167	47.51 ± 3.00	22.85	6.56	0.25 ± 0.02
1220	0.000364	0.026361	0.000013	0.006937	0.038407	49.34 ± 2.81	26.29	5.62	0.15 ± 0.00
1300	0.000457	0.037065	0.000017	0.009657	0.054049	49.87 ± 2.28	28.60	7.82	0.151 ± 0.01
1400	0.000129	0.010752	0.000003	0.002708	0.014978	49.30 ± 2.80	28.23	2.19	0.146 ± 0.00
				05122408, J = 0.0049960 ± 0.0000100					
700	0.000053	0.000982	0.000001	0.000186	0.001709	81.16 ± 20.13	9.80	0.53	0.10 ± 0.01
780	0.000216	0.014896	0.000004	0.001286	0.010300	70.94 ± 7.85	13.89	3.69	0.04 ± 0.00
840	0.000232	0.049965	0.000004	0.001691	0.014490	75.82 ± 6.61	17.45	4.86	0.02 ± 0.00
900	0.000153	0.063831	0.000001	0.003733	0.023337	55.62 ± 2.03	34.04	10.72	0.03 ± 0.00
950	0.000032	0.012663	0.000002	0.003633	0.020619	50.55 ± 0.69	68.87	10.44	0.16 ± 0.00
990	0.000019	0.007658	0.000003	0.002867	0.014844	46.17 ± 0.60	72.10	8.24	0.21 ± 0.00
1030	0.000036	0.008550	0.000001	0.004030	0.021030	46.54 ± 0.54	66.24	11.58	0.26 ± 0.01
1070	0.000039	0.007946	0.000000	0.003842	0.020016	46.47 ± 0.52	63.75	11.04	0.27 ± 0.01
1110	0.000028	0.007739	0.000000	0.003039	0.015710	46.11 ± 0.60	65.78	8.73	0.22 ± 0.00
1150	0.000030	0.013827	0.000003	0.003863	0.020149	46.52 ± 0.52	69.46	11.10	0.15 ± 0.00
1200	0.000022	0.013560	0.000001	0.002114	0.011061	46.66 ± 0.79	62.75	6.07	0.08 ± 0.00
1260	0.000021	0.013220	0.000002	0.001707	0.008995	46.99 ± 0.98	59.58	4.90	0.07 ± 0.00

Table A1. (continued)

Temperature (°C)	^{36}Ar[a][b]	^{37}Ar[Ca][b]	^{38}Ar[Cl][b]	^{39}Ar[k][b]	^{40}Ar[r][b]	Age ± 2σ (Ma)	^{40}Ar[r][b] (%)	^{39}Ar[k][b] (%)	K/Ca[c] ± 2σ
1330	0.000013	0.008450	0.000001	0.000957	0.005147	47.94 ± 1.19	56.40	2.75	0.06 ± 0.00
1400	0.000025	0.011675	0.000001	0.001864	0.009969	47.68 ± 0.76	57.64	5.35	0.09 ± 0.00
				05122602, J = 0.0049030 ± 0.0000098					
740	0.000599	0.000133	0.000015	0.001365	0.004374	28.18 ± 19.18	2.41	0.29	5.95 ± 1.630
800	0.000344	0.000336	0.000006	0.003185	0.012859	35.44 ± 4.92	11.22	0.68	5.50 ± 0.637
850	0.002637	0.000924	0.000007	0.007743	0.028431	32.26 ± 14.26	3.52	1.65	4.85 ± 0.28
890	0.001015	0.000574	0.000001	0.003957	0.012554	27.91 ± 10.87	4.02	0.84	3.99 ± 0.35
930	0.000484	0.001969	0.000008	0.013854	0.067706	42.82 ± 1.52	32.13	2.95	4.08 ± 0.13
970	0.000198	0.002193	0.000007	0.023392	0.117388	43.96 ± 0.44	66.69	4.99	6.18 ± 0.15
1010	0.000157	0.002093	0.000006	0.030601	0.154238	44.14 ± 0.30	76.88	6.53	8.48 ± 0.37
1050	0.000109	0.001282	0.000006	0.035251	0.178295	44.30 ± 0.27	84.74	7.52	15.95 ± 0.63
1100	0.000104	0.001174	0.000010	0.038997	0.197451	44.34 ± 0.24	86.46	8.32	19.26 ± 2.38
1150	0.000119	0.001814	0.000007	0.039677	0.200482	44.25 ± 0.24	85.10	8.46	12.68 ± 0.35
1200	0.000269	0.003382	0.000015	0.067511	0.340387	44.16 ± 0.28	81.04	14.40	11.57 ± 0.29
1260	0.000100	0.001145	0.000009	0.022881	0.115313	44.14 ± 0.32	79.51	4.88	11.58 ± 0.51
1320	0.000518	0.002511	0.000020	0.108353	0.551698	44.59 ± 0.30	78.26	23.11	25.02 ± 0.84
1400	0.000240	0.001172	0.000010	0.049637	0.251781	44.42 ± 0.32	78.02	10.59	24.56 ± 1.06
1500	0.000110	0.000622	0.000007	0.022526	0.114169	44.39 ± 0.35	77.84	4.80	21.01 ± 1.32
				05122605, J = 0.0050190 ± 0.0000101					
600	0.000101	0.000027	0.000000	0.000074	0.000247	30.02 ± 99.98	0.82	0.01	1.51 ± 1.65
780	0.006584	0.001179	0.000023	0.015010	0.160544	94.56 ± 18.08	7.62	1.93	7.12 ± 0.14
820	0.001181	0.000645	0.000000	0.019578	0.108990	49.83 ± 2.64	23.80	2.51	16.99 ± 0.65
870	0.000706	0.000609	0.000002	0.026802	0.145622	48.65 ± 1.16	41.11	3.44	24.63 ± 1.03
910	0.000731	0.000793	0.000009	0.031931	0.172661	48.42 ± 1.00	44.42	4.10	22.55 ± 0.59
950	0.000955	0.001389	0.000025	0.041408	0.226409	48.96 ± 1.00	44.52	5.31	16.69 ± 0.31
990	0.001225	0.002240	0.000030	0.061195	0.329223	48.18 ± 0.88	47.63	7.85	15.30 ± 0.32
1030	0.001488	0.003501	0.000047	0.098038	0.518194	47.35 ± 0.69	54.09	12.58	15.68 ± 0.27
1060	0.001143	0.004889	0.000070	0.122719	0.636037	46.44 ± 0.44	65.32	15.75	14.05 ± 0.26
1100	0.001052	0.006797	0.000088	0.139490	0.718901	46.18 ± 0.38	69.80	17.90	11.49 ± 0.21
1150	0.000763	0.005218	0.000078	0.104626	0.537952	46.07 ± 0.38	70.47	13.43	11.22 ± 0.22
1210	0.000516	0.003547	0.000082	0.056842	0.289176	45.59 ± 0.47	65.48	7.29	8.97 ± 0.20
1300	0.000347	0.002628	0.000065	0.029873	0.147944	44.40 ± 0.55	59.07	3.83	6.36 ± 0.15
1400	0.000266	0.002066	0.000053	0.031673	0.154157	43.64 ± 0.47	66.23	4.06	8.58 ± 0.14

[a] Age of the fluence monitor Bern 4M is 18.7 ± 0.1 Ma [*Hall et al.*, 1984].
[b] ^{36}Ar[a], ^{37}Ar[Ca], ^{38}Ar[Cl], ^{39}Ar[k], and ^{40}Ar[r] denote the atmospheric ^{36}Ar, ^{37}Ar derived from Ca, ^{38}Ar derived from Cl, ^{39}Ar derived from k, and radiogenic ^{40}Ar in mV, respectively.
[c] K/Ca = [^{39}Ar[k]/^{37}Ar[Ca]] * 0.56 [*Wang et al.*, 2006a].

Table A2. Compilation of Published Age Data and Data in This Study on the South Shetland Islands[a]

Locality	Lithology	Age ± 2σ	Method	Reference
President Head, Snow I.	dacite	46 ± 2	K-Ar	*Pankhurst and Smellie* [1983]
Ray Promontory, Byers P., Livingston I.	andesite dike	128 ± 4	K-Ar	
	basalt sill	123 ± 5	K-Ar	
Chester Cove, Byers P., Livingston I.	andesite plug	110 ± 4	K-Ar	
	andesite plug	113 ± 4	K-Ar	
	andesite plug	132 ± 5	K-Ar	
	rhyolite	109 ± 4	K-Ar	
Vietor Rock, Byers P., Livingston I.	basalt	106 ± 4	K-Ar	
	basaltic andesite	108 ± 4	K-Ar	
	basaltic andesite	86 ± 3	K-Ar	
Sealer Hill, Byers P., Livingston I.	dolerite plug	108 ± 4	K-Ar	
	dolerite plug	109 ± 4	K-Ar	
Eastern Byers P., Livingston I.	basalt	94 ± 3	K-Ar	
	basalt	79 ± 3	K-Ar	
	basalt sill	76 ± 3	K-Ar	
	basalt sill	77 ± 3	K-Ar	
	basalt sill	74 ± 3	K-Ar	
Negro Hill, E. Byers P., Livingston I.	dolerite plug	89 ± 4	K-Ar	
	dolerite plug	95 ± 5	K-Ar	
Sayer Nunatak, Livingston I.	basalt sill	74 ± 2	K-Ar	
	basalt sill	79 ± 2	K-Ar	
	clast in vent	81 ± 2	K-Ar	
Barnard Point, Livingston I.	tonite	40 ± 1	K-Ar	
	tonite	46 ± 2	K-Ar	
	basalt	0.1 ± 0.4	K-Ar	
Express I.	gabbro	84 ± 2	K-Ar	
Greenwich	basalt sill	80 ± 2	K-Ar	
	basalt	0.2 ± 0.3	K-Ar	
	basalt	0.2 ± 0.4	K-Ar	
Coppermine P., Robert I.	basalt	82 ± 2	K-Ar	
	basalt	83 ± 3	K-Ar	
	basalt	80 ± 2	K-Ar	
	basalt	84 ± 2	K-Ar	
	basalt	82 ± 3	K-Ar	
	gabbro	60 ± 1	K-Ar	
Kitchen Point, Robert I.	andesite	53 ± 1	K-Ar	
South Fildes P., King George I.	andesite	51 ± 1	K-Ar	
	andesite	59 ± 2	K-Ar	
	andesite	58 ± 1	K-Ar	
	andesite	58 ± 2	K-Ar	
	altered lava	58 ± 1	K-Ar	
	altered lava	31 ± 3	K-Ar	
Horatio, King George I.	andesite plug	51 ± 1	K-Ar	
Northern Fildes P., King George I.	andesite	58 ± 4	K-Ar	
	basalt	52 ± 1	K-Ar	
	basalt	48 ± 1	K-Ar	
	basalt	48 ± 1	K-Ar	
	basalt	57 ± 3	K-Ar	
	basaltic andesite	43 ± 1	K-Ar	
	dacite	42 ± 1	K-Ar	
	dacite	46 ± 1	K-Ar	
	andesite plug	44 ± 1	K-Ar	
Marian Cove, King George I.	basaltic andesite	46 ± 1	K-Ar	
Potter P., King George I.	basalt	44 ± 1	K-Ar	
	basaltic andesite	45 ± 1	K-Ar	
	basaltic andesite	42 ± 1	K-Ar	
	basaltic andesite	47 ± 1	K-Ar	
	andesite	48 ± 1	K-Ar	
Three Brothers Hill, King George I.	andesite plug	47 ± 1	K-Ar	
Noel Hill, King George I.	granodiorite plug	48 ± 1	K-Ar	
	granodiorite	46 ± 1	K-Ar	

Table A2. (continued)

Locality	Lithology	Age ± 2σ	Method	Reference
Point Hennequin, King George I.	andesite	45 ± 1	K-Ar	
	andesite	27 ± 1	K-Ar	
	andesite	32 ± 1	K-Ar	
	andesite	46 ± 1	K-Ar	
	andesite	47 ± 1	K-Ar	
Keller P., King George I.	andesite dike	41 ± 1	K-Ar	
	andesite dike	44 ± 1	K-Ar	
	andesite dike	42 ± 1	K-Ar	
Lion's Rump, King George I.	andesite	42 ± 1	K-Ar	
Esther Nunatak, King George I.	andesite	32 ± 1	K-Ar	
Hurd P., Livingston I.	andesite dike	66.8 ± 2.0	K-Ar	*Willan and Kelley* [1999]
	basalt dike	50.8 ± 1.5	K-Ar	
	andesite dike	48.0 ± 2.0	K-Ar	
	basalt-andesite dike	45.0 ± 2.0	K-Ar	
	basalt dike	45.4 ± 2.0	K-Ar	
	basalt-andesite dike	47.5 ± 1.5	K-Ar	
Barnard Point, Livingston I.	andesite dike	40.3 ± 2.0	K-Ar	
	basalt dike	35.6 ± 1.5	K-Ar	
	andesite dike	31.0 ± 1.0	K-Ar	
	andesite dike	28.6 ± 1.0	K-Ar	
Wegger P., Admiralty Bay, King George I.	diorite	43.5 ± 4.8	K-Ar	*Birkenmajer et al.* [1986]
	quartz diorite	43.7 ± 9.5	K-Ar	
Admiralen P., Admiralty Bay, King George I.	basaltic andesite	43.7 ± 4.8	K-Ar	
Keller P., Admiralty Bay, King George I.	andesite	44.1 ± 4.3	K-Ar	
	basaltic andesite	26.4 ± 2.6	K-Ar	
	basaltic andesite	39.9 ± 3.4	K-Ar	
Cape Melville, King George I.	basaltic dike	23.0 ± 1.4	K-Ar	*Birkenmajer et al.* [1989]
Cinder Spur, King George I.	basaltic dike	21.9 ± 1.1	K-Ar	
Harnasie Hill, King George I.	basaltic dike	30.5 ± 5.5	K-Ar	
Dunikowski Ridge, King George I.	andesite	30.8 ± 2.0	K-Ar	
Cape Vaureal, King George I.	andesite	33.4 ± 7.0	K-Ar	
Vaureal P., King George I.	andesite	17.3 ± 1.3	K-Ar	
Mersey Spit, King George I.	basaltic andesite	34.3 ± 0.5	K-Ar	
Mersey Spit, King George I.	andesite plug	37.6 ± 0.9	K-Ar	
Cape Vaureal, King George I.	andesite plug	45.9 ± 0.7	K-Ar	
Vaureal P., King George I.	andesite	47.0 ± 1.1	K-Ar	
Puchalski P., King George I.	andesite dike	49.0 ± 5.5	K-Ar	
Southern end of Hurd P., Livingston I.	diorite	73.0 ± 3.0	K-Ar	*Kamenov* [1997]
	granodiorite	40.0 ± 2.0	K-Ar	
Burdick Pk., Livingston I.	basalt	0.04 ± 0.35	K-Ar	*Smellie et al.* [1996]
Samuel Pk., Livingston I.	basalt	0.70 ± 0.35	K-Ar	
Willan Nunatak, Livingston I.	tonalite	41.4 ± 1.3	K-Ar	
	tonalite	43.3 ± 2.8	K-Ar	
Moores Pk., Livingston I.	basalt	35.0 ± 3.9	K-Ar	
Willan Nunatak, Livingston I.	andesite	44.4 ± 1.3	K-Ar	
Mt Bowles, Livingston I.	basaltic andesite	39.8 ± 1.6	K-Ar	
Siddons Point, Livingston I.	dolerite	73.0 ± 2.3	K-Ar	
Hannah Point, Livingston I.	basaltic andesite	67.5 ± 2.5	K-Ar	
	basaltic andesite	87.9 ± 2.6	K-Ar	
Cape Shirreff, Livingston I.	basalt	90.2 ± 5.6	K-Ar	
Hurd P., Livingston I.	diorite	73.8 ± 13.0	$^{40}Ar/^{39}Ar$ isochron	*Willan and Kelley* [1999]
	basaltic andesite	40.5 ± 1.1	$^{40}Ar/^{39}Ar$ isochron	
	gabbro	48.5 ± 1.8	$^{40}Ar/^{39}Ar$ isochron	
	gabbro	47.4 ± 0.6	$^{40}Ar/^{39}Ar$ isochron	
	basalt-andesite dike	45.3 ± 5.2	$^{40}Ar/^{39}Ar$ isochron	
	basalt dike	41.6 ± 2.1	$^{40}Ar/^{39}Ar$ isochron	
	pegmatite	29.3 ± 0.7	$^{40}Ar/^{39}Ar$ isochron	
	trachybasalt	78.8 ± 1.8	K-Ar	*Zheng et al.* [2003]
	Hawaiite	63.7 ± 1.3	K-Ar	
	dacite	62.0 ± 2.0	K-Ar	
	basalt	61.0 ± 2.1	K-Ar	
	latite	52.5 ± 1.5	K-Ar	

Table A2. (continued)

Locality	Lithology	Age ± 2σ	Method	Reference
	basaltic andesite	53.5 ± 1.6	K-Ar	
	andesite	44.5 ± 2.0	K-Ar	
	andesite	42.0 ± 2.1	K-Ar	
	trachybasalt	43.5 ± 2.5	K-Ar	
	basalt	44.5 ± 2.2	K-Ar	
	andesite	44.0 ± 2.0	K-Ar	
	shoshonite	43.0 ± 1.8	K-Ar	
	dacite	38.0 ± 2.0	K-Ar	
	basalt	34.0 ± 1.9	K-Ar	
	leucobasalt	31.0 ± 2.2	K-Ar	
	basalt	55.4 ± 0.6	$^{40}Ar/^{39}Ar$ isochron	
	basalt	64.9 ± 0.4	$^{40}Ar/^{39}Ar$ isochron	
	basalt	52.7 ± 0.2	$^{40}Ar/^{39}Ar$ isochron	
Admiralty Bay, King George I.	basalt dike	45.4 ± 0.6	$^{40}Ar/^{39}Ar$ isochron	*Kraus* [2005]
	andesite	47.1 ± 0.6	$^{40}Ar/^{39}Ar$ isochron	
	basalt dike	54.0 ± 1.5	$^{40}Ar/^{39}Ar$ isochron	
Potter P., King George I.	rhyolite dike	45.7 ± 1.2	$^{40}Ar/^{39}Ar$ isochron	
	andesite dike	46.4 ± 0.6	$^{40}Ar/^{39}Ar$ isochron	
	andesite dike	46.6 ± 0.4	$^{40}Ar/^{39}Ar$ isochron	
	andesite dike	47.0 ± 0.6	$^{40}Ar/^{39}Ar$ isochron	
	basalt dike	47.2 ± 0.5	$^{40}Ar/^{39}Ar$ isochron	
Weaver P., King George I.	andesite	54.6 ± 3.8	$^{40}Ar/^{39}Ar$ isochron	
Fildes P., King George I.	andesite	57.4 ± 2.1	$^{40}Ar/^{39}Ar$ isochron	
Hurd P., Livingston I.	andesite	37.2 ± 0.9	$^{40}Ar/^{39}Ar$ isochron	
	andesite	39.8 ± 7.3	$^{40}Ar/^{39}Ar$ isochron	
	andesite	48.3 ± 1.5	$^{40}Ar/^{39}Ar$ isochron	
	dacite	53 ± 16	$^{40}Ar/^{39}Ar$ isochron	
	dacite	64 ± 13	$^{40}Ar/^{39}Ar$ isochron	
	dacite	43.3 ± 1.7	K-Ar	
	basaltic andesite	44.5 ± 1.8	K-Ar	
	andesite	47.4 ± 2.1	K-Ar	
	andesite	56.5 ± 2.3	K-Ar	
	dacite	80.1 ± 3.1	K-Ar	
Moore Peak, Hurd P., Livingston I.	gabbro	45.0 ± 3.8	$^{40}Ar/^{39}Ar$ isochron	*Kamenov et al.* [2005]
Cerro Mirador, Hurd P., Livingston I.	granodiorite	44.9 ± 2.3	$^{40}Ar/^{39}Ar$ isochron	
Barton P., King George I.	andesite	44.2 ± 1.6	$^{40}Ar/^{39}Ar$ isochron	this study
Weaver P., King George I.	mafic dike	43.9 ± 1.5	$^{40}Ar/^{39}Ar$ isochron	
	mafic dike	44.6 ± 0.8	$^{40}Ar/^{39}Ar$ isochron	
	diorite	44.0 ± 1.4	$^{40}Ar/^{39}Ar$ isochron	
	basalt	45.8 ± 1.7	$^{40}Ar/^{39}Ar$ isochron	
	mafic dike	44.6 ± 1.1	$^{40}Ar/^{39}Ar$ isochron	
Barton P., King George I.	granodiorite	44.5 ± 0.3	$^{40}Ar/^{39}Ar$ isochron	
	propylite	44.8 ± 0.6	$^{40}Ar/^{39}Ar$ isochron	

[a] Data are summarized from *Pankhurst and Smellie* [1983], *Smellie et al.* [1984], *Birkenmajer et al.* [1986], *Smellie et al.* [1996], *Kamenov* [1997], *Willan and Kelley* [1999], *Zheng et al.* [2003], *Kraus* [2005], *Kamenov et al.* [2005], and this study.

and $^{40}Ar[r]$ denote the atmospheric ^{36}Ar, ^{37}Ar derived from Ca, ^{38}Ar derived from Cl, ^{39}Ar derived from k and radiogenic ^{40}Ar in mV, respectively; K/Ca ratios are calculated by using $K/Ca = [^{39}Ar[k]/^{37}Ar[Ca]] * 0.56$ [*Wang et al.*, 2006a]. The fluence monitor in this work is Bern 4M with calibrated age of 18.7 ± 0.1 Ma [*Hall et al.*, 1984]. Compilation of published ages on the South Shetland Islands is shown in Table A2. Data are summarized from *Pankhurst and Smellie* [1983], *Smellie et al.* [1984], *Birkenmajer et al.* [1986], *Smellie et al.* [1996], *Kamenov* [1997], *Willan and Kelley* [1999], *Zheng et al.* [2003], *Kraus* [2005], *Kamenov et al.* [2005], and this study.

Acknowledgments

[72] We thank A. A. P. Koppers and an anonymous reviewer for their thorough and helpful reviews that have significantly improved the manuscript. This work was supported by KOPRI projects (PE09020 and PP09030) and Chinese Science Foundation (40221402, 40873046, 40672056, and 90714007).

References

Alabaster, T., and B. C. Storey (1990), Antarctic Peninsula magnesian andesites: Indicators of ridge-trench interaction during Gondwana break-up, *J. Geol. Soc.*, *147*, 595–598, doi:10.1144/gsjgs.147.4.0595.

Aldaya, F., and A. Madonado (1996), Tectonics of the triple junction at the southern end of the Shackleton Fracture Zone (Antarctic Peninsula), *Geo Mar. Lett.*, *16*, 279–286, doi:10.1007/BF01245558.

Baksi, A. K. (1974), Isotopic fractionation of a loosely held atmospheric argon component in the Picture Gorge basalts, *Earth Planet. Sci. Lett.*, *21*, 431–438, doi:10.1016/0012-821X(74)90183-6.

Barker, P. F. (1982), The Cenozoic subduction history of the Pacific margin of the Antarctic Peninsula: Ridge crest-trench interactions, *J. Geol. Soc.*, *139*, 787–801, doi:10.1144/gsjgs.139.6.0787.

Bird, P. (1979), Continental delamination and the Colorado Plateau, *J. Geophys. Res.*, *84*, 7561–7571.

Birkenmajer, K. (1994), Evolution of the Pacific margin of the northern Antarctic Peninsula: A overview, *Geol. Rundsch.*, *83*, 309–321.

Birkenmajer, K., M. C. Delitala, W. Narebski, M. Nicoletti, and C. Petrucciani (1986), Geochronology and migration of Cretaceous through Tertiary plutonic centers, South Shetlands (West Antarctica): Subduction and hot spot magmatism, *Bull. Pol. Acad. Sci. Earth Sci.*, *34*, 243–255.

Birkenmajer, K., E. Soliani, and J. K. Kawashita (1989), Geochronology of Tertiary glaciations on King George Island, West Antarctica, *Bull. Pol. Acad. Sci. Earth Sci.*, *37*, 28–48.

Carroll, M. R. (1991), Diffusion of Ar in rhyolite, orthoclase and albite composition glasses, *Earth Planet. Sci. Lett.*, *103*, 156–168, doi:10.1016/0012-821X(91)90157-D.

Chen, D., M. Jia, B. Li, Q. Lu, H. Xie, and W. Hou (1995), Argon diffusion from biotite at high temperature and pressure, *Sci. China, Ser. B*, *38*, 221–227.

Dalrymple, G. B., and D. A. Clague (1976), Age of the Hawaiian–Emperor bend, *Earth Planet. Sci. Lett.*, *31*, 313–329, doi:10.1016/0012-821X(76)90113-8.

Davis, R. E. S. (1982), The geology of the Marian Cove area, King George Island and a Tertiary age for its supposed Jurassic volcanic rocks, *Br. Antarct. Surv. Bull.*, *51*, 151–165.

Delong, S. E., W. M. Schwarz, and R. N. Anderson (1979), Thermal effects of ridge subduction, *Earth Planet. Sci. Lett.*, *44*, 239–246, doi:10.1016/0012-821X(79)90172-9.

Dupre, D. D. (1982), Geochemistry and $^{40}Ar/^{39}Ar$ geochronology of some igneous rocks from the South Islands, Antarctica, M.Sc. thesis, 229 pp., Ohio State Univ., Columbus.

England, P. C., and P. Molnar (1990), Surface uplift, uplift of rocks, and exhumation of rocks, *Geology*, *18*, 1173–1177, doi:10.1130/0091-7613(1990)018<1173:SUUORA>2.3.CO;2.

Fleck, R. J., J. F. Sutter, and D. H. Elliot (1977), Interpretation of discordant $^{40}Ar/^{39}Ar$ age-spectra of Mesozoic tholeiites from Antarctica, *Geochim. Cosmochim. Acta*, *41*, 15–32, doi:10.1016/0016-7037(77)90184-3.

Foland, K. A., T. H. Fleming, A. Heimann, and D. H. Elliot (1993), Potassium-argon dating of fine-grained basalts with massive Ar loss: Application of the $^{40}Ar/^{39}Ar$ technique to plagioclase and glass from the Kirkpatrick Basalts, Antarctica, *Chem. Geol.*, *107*, 173–190, doi:10.1016/0009-2541(93)90109-V.

Galindo-Zaldívar, J., L. Gamboa, A. Maldonado, S. Nakao, and B. Yao (2004), Tectonic development of the Bransfield Basin and its prolongation to the South Scotia Ridge, northern Antarctic Peninsula, *Mar. Geol.*, *206*, 267–282, doi:10.1016/j.margeo.2004.02.007.

Gracanin, T. M. (1983), Geochemistry and geochronology of some Mesozoic igneous rocks from the northern Antarctic Peninsula region, M.Sc. thesis, 193 pp., Ohio State Univ., Columbus.

Hall, C. M., R. C. Walter, J. A. Westgate, and D. York (1984), Geochronology, stratigraphy and geochemistry of Cindery Tuff in Pliocene hominid-bearing sediments of the Middle Awash, Ethiopia, *Nature*, *308*, 26–31, doi:10.1038/308026a0.

Henriet, J. P., R. Meissner, H. Miller, and the GRAPE Team (1992), Active margin processes along the Antarctic Peninsula, *Tectonophysics*, *201*, 229–253, doi:10.1016/0040-1951(92)90235-X.

Hur, S. D., J. I. Lee, J. Hwang, and M. Y. Choe (2001), K-Ar age and geochemistry of hydrothermal alteration in the Barton Peninsula, King George Island, Antarctica, *Ocean Polar Res.*, *23*, 11–21.

Kamenov, B. K. (1997), Geochemistry and petrology of the Hesperides point intrusion, Hurd Peninsula, Livingston Island, in *The Antarctic Region: Geological Evolution and Processes*, edited by C. Ricci, pp. 341–352, Terra Antarct., Siena, Italy.

Kamenov, B. K., X. Zheng, D. Dimov, and C. Pimpire (2005), The isolated plutons in Hurd Peninsula, Livingston Island, Antarctica: Petrological and geochronological evidences of their affiliations to Barnard Point Batholith, *Geochem. Mineral. Petrol.*, *42*, 67–86.

Kelley, S. P., and J.-A. Wartho (2000), Rapid kimberlite ascent and the significance of Ar-Ar ages in xenolith phlogopites, *Science*, *289*, 609–611, doi:10.1126/science.289.5479.609.

Kim, H., J. I. Lee, M. Y. Choe, M. Cho, X. Zheng, H. Sang, and J. Qiu (2000), Geochronologic evidence for Early Cretaceous volcanic activity on Barton Peninsula, King George Island, Antarctica, *Polar Res.*, *19*, 251–260, doi:10.1111/j.1751-8369.2000.tb00347.x.

Koppers, A. A. P. (2002), ArArCALC—Software for $^{40}Ar/^{39}Ar$ age calculations, *Comput. Geosci.*, *28*, 605–619, doi:10.1016/S0098-3004(01)00095-4.

Koppers, A. A. P., and H. Staudigel (2003), High-resolution $^{40}Ar/^{39}Ar$ dating of the oldest oceanic basement basalts in the western Pacific basin, *Geochem. Geophys. Geosyst.*, *4*(11), 8914, doi:10.1029/2003GC000574.

Koppers, A. A. P., H. Staudigel, and J. R. Wijbrans (2000), Dating crystalline groundmass separates of altered Cretaceous seamount basalts by the $^{40}Ar/^{39}Ar$ incremental heating technique, *Chem. Geol.*, *166*, 139–158, doi:10.1016/S0009-2541(99)00188-6.

Kraus, S. (2005), Magmatic dyke systems of the South Shetland Islands volcanic arc (West Antarctica): Reflections of the geodynamic history, Als dissertation, 66 pp., Ludwig-Maximilians Univ., Munich, Germany.

Lawver, L. A., L. M. Gahagan, and M. F. Coffin (1992), The development of paleoseaways around Antarctica, in *The Antarctic Paleoenvironment: A Perspective on Global Change*, *Antarct. Res. Ser.*, vol. 10, edited by J. P. Kennett and D. A. Warke, pp. 1038–1064, AGU, Washington, D. C.

Lee, J. I., J. Hwang, H. Kim, C. Y. Kang, M. J. Lee, and K. Nagao (1996), Subvolcanic zoned granitic pluton in the Barton and Weaver peninsulas, King George Island, Antarctica, *Proc. NIPR Symp. Antarct. Geosci.*, *9*, 76–90.

Lee, J. I., et al. (2002), Geological map of Barton and Weaver peninsulas, King George Island, Antarctica, 30 pp., Korea Ocean Res. and Dev. Inst., Ansan, South Korea.

Lee, M. J., J. I. Lee, W. H. Choe, and C. H. Park (2008), Trace element and isotopic evidence for temporal changes of the mantle sources in the South Shetland Islands, Antarctica, *Geochem. J.*, *42*, 207–219.

Livermore, R., et al. (2000), Autopsy on a dead spreading centre: The Phoenix Ridge, *Geology*, *28*, 607–610, doi:10.1130/0091-7613(2000)28<607:AOADSC>2.0.CO;2.

Lo, C. H., T. C. Onstott, C. H. Chen, and T. Lee (1994), An assessment of $^{40}Ar/^{39}Ar$ dating of the whole-rock volcanic samples from the Luzon Arc near Taiwan, *Chem. Geol.*, *114*, 157–178, doi:10.1016/0009-2541(94)90049-3.

Maldonado, A., R. D. Larter, and F. Aldaya (1994), Forearc tectonic evolution of the South Shetland margin, Antarctic Peninsula, *Tectonics*, *13*, 1345–1370, doi:10.1029/94TC01352.

Maldonado, A., et al. (2000), Tectonics of an extinct ridge transform intersection, Drake Passage (Antarctica), *Mar. Geophys. Res.*, *21*, 43–68, doi:10.1023/A:1004762311398.

Maurel, O., P. Monie, J. P. Respaut, A. F. Leyreloup, and H. Maluski (2003), Pre-metamorphic $^{40}Ar/^{39}Ar$ and U-Pb ages in HP metagranitoids from the Hercynian belt (France), *Chem. Geol.*, *193*, 195–214, doi:10.1016/S0009-2541(02)00351-0.

McCarron, J. J., and R. D. Larter (1998), Late Cretaceous to early Tertiary subduction history of the Antarctic Peninsula, *J. Geol. Soc.*, *155*, 255–268, doi:10.1144/gsjgs.155.2.0255.

McCarron, J. J., and I. L. Millar (1997), The age and stratigraphy of fore-arc magmatism on Alexander Island, Antarctica, *Geol. Mag.*, *134*, 507–522.

McDougall, I., and T. M. Harrison (1999), *Geochronology and Thermochronology by the $^{40}Ar/^{39}Ar$ Method*, 123 pp., Oxford Univ. Press, New York.

Pankhurst, R. J., and J. L. Smellie (1983), K-Ar geochronology of the South Shetland Islands, Lesser Antarctica: Apparent lateral migration of Jurassic to Quaternary island arc volcanism, *Earth Planet. Sci. Lett.*, *66*, 214–222, doi:10.1016/0012-821X(83)90137-1.

Park, B.-K. (1989), Potassium-argon radiometric ages of volcanic and plutonic rocks from the Barton Peninsula, King George Island, Antarctica, *J. Geol. Soc. Korea*, *25*, 495–497.

Pelayo, A. M., and D. A. Wiens (1989), Seismotectonics and relative plate motions in the Scotia Sea region, *J. Geophys. Res.*, *94*, 7293–7320, doi:10.1029/JB094iB06p07293.

Pringle, M. S. (1993), Age progressive volcanism in the musicians seamounts: A test of the hot spot hypothesis for the late Cretaceous Pacific, in *The Mesozoic Pacific: Geology, Tectonics, and Volcanism*, *Geophys. Monogr. Ser.*, vol. 77, edited by M. S. Pringle et al., pp. 187–216, AGU, Washington, D. C.

Roddick, J. C. (1978), The application of isochron diagrams in $^{40}Ar/^{39}Ar$ dating: A discussion, *Earth Planet. Sci. Lett.*, *41*, 233–244, doi:10.1016/0012-821X(78)90014-6.

Scarrow, J. H., P. T. Leat, C. D. Wareham, and I. L. Millar (1998), Geochemistry of mafic dykes in the Antarctic Peninsula continental-margin batholith: A record of arc evolution, *Contrib. Mineral. Petrol.*, *131*, 289–305, doi:10.1007/s004100050394.

Seidemann, D. E. (1977), Effects of submarine alteration on K–Ar dating of deep-sea igneous rocks, *Geol. Soc. Am. Bull.*, *88*, 1660–1666, doi:10.1130/0016-7606(1977)88<1660:EOSAOK>2.0.CO;2.

Seidemann, D. E. (1978), $^{40}Ar/^{39}Ar$ studies of deep-sea igneous rocks, *Geochim. Cosmochim. Acta*, *42*, 1721–1734, doi:10.1016/0016-7037(78)90258-2.

Seidemann, D. E. (1988), The hydrothermal addition of excess ^{40}Ar to the lava flows from the Early Jurassic in the Hartford basin, northeastern U.S.A.: Implications for the time scale, *Chem. Geol.*, *72*, 37–45.

Sieminski, A., E. Debayle, and J. J. Leveque (2003), Seismic evidence for deep low-velocity anomalies in the transition zone beneath West Antarctica, *Earth Planet. Sci. Lett.*, *216*, 645–661, doi:10.1016/S0012-821X(03)00518-1.

Singer, B. S., and M. S. Pringle (1996), Age and duration of the Matuyama–Brunhes geomagnetic polarity reversal from $^{40}Ar/^{39}Ar$ incremental heating analyses of lavas, *Earth Planet. Sci. Lett.*, *139*, 47–61, doi:10.1016/0012-821X(96)00003-9.

Singer, B. S., J. R. Wijbrans, S. T. Nelson, M. S. Pringle, T. C. Feely, and M. A. Dungan (1998), Inherited argon in a Pleistocene andesite lava: $^{40}Ar/^{39}Ar$ incremental-heating and laser-fusion analyses of plagioclase, *Geology*, *26*, 427–430, doi:10.1130/0091-7613(1998)026<0427:IAIAPA>2.3.CO;2.

Smellie, J. L., R. J. Pankhurst, M. R. A. Thomson, and R. E. S. Davies (1984), The geology of the South Shetland Islands IV: Stratigraphy, geochemistry and evolution, *Br. Ant. Surv. Sci. Rep.*, *87*, 1–83.

Smellie, J. L., R. Pallàs, F. Sabat, and X. Zheng (1996), Age and correlation of volcanism in central Livingston Island, South Shetland Islands: K-Ar and geochemical constraints, *J. South Am. Earth Sci.*, *9*, 265–272, doi:10.1016/0895-9811(96)00012-0.

Steiger, R. H., and E. Jäger (1977), Subcommision on Geochronology: Convention on the use of decay constants in geo- and cosmochronology, *Earth Planet. Sci. Lett.*, *36*, 359–362, doi:10.1016/0012-821X(77)90060-7.

Storey, B. C., and T. Alabaster (1991), Tectonomagmatic controls on Gondwana break-up models: Evidence from the proto-Pacific margin of Antarctica, *Tectonics*, *10*, 1274–1288, doi:10.1029/91TC01122.

Storey, B. C., A. P. M. Vaughan, and I. L. Millar (1996), Geodynamic evolution of the Antarctic Peninsula during Mesozoic times and its bearing on Weddell Sea history, in *Weddell Sea Tectonics and Gondwana Break-Up*, edited by B. C. Storey, R. L. Livermore, and E. C. King, *Geol. Soc. Spec. Publ.*, *108*, 87–103.

Sun, S. S., and W. F. McDonough (1989), Chemical and isotopic systematics of oceanic basalts: Implications for mantle composition and processes, in *Magmatism in the Ocean Basins*, edited by A. D. Saunders and M. J. Norry, *Geol. Soc. Spec. Publ.*, *42*, 313–345.

Tatsumi, Y., and S. Eggins (1995), *Subduction Zone Magmatism*, 211 pp., Blackwell Sci., Cambridge, Mass.

Taylor, T. J. R. (1997), *An Introduction to Error Analysis: The Study of Uncertainties in Physical Measurements*, 327 pp., Univ. Sci. Books, Mill Valley, Calif.

Trouw, R. A. J., L. S. A. Simoes, and C. S. Valladares (1998), Metamorphic evolution of a subduction complex, South Shetland Islands, Antarctica, *J. Metamorph. Geol.*, *16*, 475–490, doi:10.1111/j.1525-1314.1998.00151.x.

Turner, G., and P. H. Cadogan (1974), Possible effects of ^{39}Ar recoil in $^{40}Ar/^{39}Ar$ dating of lunar samples, *Proc. Lunar Sci. Conf.*, *5th*, 1601–1615.

Turner, S. P., J. P. Platt, R. M. M. George, S. P. Kelley, D. G. Pearson, and G. M. Nowell (1999), Magmatism association with orogenic collapse of the Betic-Alboran Domain, SE Spain, *J. Petrol.*, *40*, 1011–1036, doi:10.1093/petrology/40.6.1011.

Walker, D. A., and I. McDougall (1982), $^{40}Ar/^{39}Ar$ and K–Ar dating of altered glassy volcanic rocks: The Dabi volcanics, *Geochim. Cosmochim. Acta*, *46*, 2181–2190, doi:10.1016/0016-7037(82)90193-4.

Wang, F., H. He, R. Zhu, H. Sang, Y. Wang, and L. Yang (2006a), Intercalibration of international and domestic $^{40}Ar/^{39}Ar$ dating standards, *Sci. China, Ser. D*, *49*, 461–470, doi:10.1007/s11430-006-0461-y.

Wang, F., X. Zhou, L. Zhang, J. Ying, Y. Zhang, F. Wu, and R. Zhu (2006b), Late Mesozoic volcanism in the Great Xing'an Range (NE China): Timing and implications for the dynamic setting of NE Asia, *Earth Planet. Sci. Lett.*, *251*, 179–198, doi:10.1016/j.epsl.2006.09.007.

Wang, F., R. Zhu, L. Yang, H. He, and C. Lo (2008), $^{40}Ar/^{39}Ar$ analyses on Quaternary K-Ar standard BB-24: Evaluations, *Int. J. Mass Spectrom.*, *270*, 16–22, doi:10.1016/j.ijms.2007.11.002.

Willan, R. C. R., and S. P. Kelley (1999), Mafic dike swarms in the South Shetland Islands volcanic arc: Unraveling mutiepisodic magmatism related to subduction and continental rifting, *J. Geophys. Res.*, *104*, 23,051–23,068, doi:10.1029/1999JB900180.

Yeo, J. P., J. I. Lee, S. D. Hur, and B. Choi (2004), Geochemistry of volcanic rocks in Barton and Weaver peninsulas, King George Island, Antarctica: Implications for arc maturity and correlation with fossilized volcanic centers, *Geosci. J.*, *8*, 11–25, doi:10.1007/BF02910275.

Yoo, C. M., M. Y. Choe, H. R. Jo, Y. Kim, and K. H. Kim (2001), Volcaniclastic sedimentation of the Sejong Formation (Late Paleocene-Eocene), Barton Peninsula, King George Island, Antarctica, *Ocean Polar Res.*, *23*, 97–107.

York, D. (1968), Least squares fitting of a straight line with correlated errors, *Earth Planet. Sci. Lett.*, *5*, 320–324, doi:10.1016/S0012-821X(68)80059-7.

Zheng, X., S. Hu, and J. Liu (1997), New $^{40}Ar/^{39}Ar$ age evidence for the Cretaceous volcanism rocks of the Mount Bowles Formation in Livingston Island, South Shetland Islands, Chin, *J. Polar Sci.*, *8*, 89–95.

Zheng, X., H. Sang, J. Qiu, and J. Liu (2000), New discovery of the Early Cretaceous volcanic rocks on the Barton Peninsula, King George Island, Antarctica and its geological significance, *Acta Geol. Sin.*, *74*, 176–182.

Zheng, X., B. Kamenov, H. Sang, and P. Monchev (2003), New radiometric dating of the dykes from the Hurd Peninsula, Livingston Island, South Shetland Islands, *J. South Am. Earth Sci.*, *15*, 925–934.